

On the missing-momentum dependence of the color-transparency effects in $(e, e' p)$ scattering

O. Benhar

INFN, Sezione Sanità, Physics Laboratory, Istituto Superiore di Sanità, I-00161 Roma, Italy

S. Fantoni

Interdisciplinary Laboratory, SISSA, INFN, Sezione di Trieste, I-34014 Trieste, Italy and International Centre for Theoretical Physics, Strada Costiera 11, I-34014 Trieste, Italy

N. N. Nikolaev

IKP(Theorie), Forschungszentrum Jülich GmbH, D-52425 Jülich, Germany and ITKP der Universität Bonn, Nußallee 14-16, D53115 Bonn, Germany and L. D. Landau Institute for Theoretical Physics, GSP-1, 117940 Moscow, Russia

J. Speth

IKP(Theorie), Forschungszentrum Jülich GmbH, D-52425 Jülich, Germany and ITKP der Universität Bonn, Nußallee 14-16, D53115 Bonn, Germany

A. A. Usmani

Interdisciplinary Laboratory, SISSA, INFN, Sezione di Trieste, I-34014 Trieste, Italy

B. G. Zakharov

L. D. Landau Institute for Theoretical Physics, GSP-1, 117940 Moscow, Russia

(Submitted 16 May 1996)

Zh. Éksp. Teor. Fiz. **110**, 1933–1959 (December 1996)

We explore the missing-momentum dependence of the color transparency (CT) effects in quasielastic $(e, e' p)$ scattering. We develop the coupled-channel multiple-scattering theory (CCMST) description of final-state interaction including both the coherent and incoherent rescatterings of the ejectile state. We demonstrate that the contribution of the off-diagonal incoherent rescattering does not vanish at low Q^2 , which is a novel correction to the conventional Glauber theory evaluation of nuclear transparency. We comment on the nontrivial impact of this correction on the onset of CT. The sensitivity of the onset of CT to the $3q$ -nucleon reggeon amplitudes is discussed for the first time. We present numerical results for nuclear transparency as a function of the missing momentum for exclusive $(e, e' p)$ reaction in the kinematical region of $Q^2 \lesssim 40 \text{ GeV}^2$ and $p_m \lesssim 250 \text{ MeV}/c$. Our evaluations show that at $Q^2 \sim 10$ CT effects are substantial only in antiparallel kinematics at $p_{m,z} \sim -250 \text{ MeV}/c$. The effect is enhanced on light nuclei and could be observed in a high-precision experiment. © 1996 American Institute of Physics. [S1063-7761(96)00212-0]

1. INTRODUCTION

The quasi-elastic $(e, e' p)$ reaction plays an important role in nuclear physics as a tool for investigating nuclear structure. At high Q^2 it becomes interesting from the point of view of the particle physics as well. Perturbative QCD¹ suggests that the dominant mechanism of ep scattering at high Q^2 is an interaction of the virtual photon with a small-size ($\rho \sim 1/Q$) $3q$ configuration in the proton wave function. It is expected^{2,3} that this mechanism should manifest itself through vanishing of the final-state interaction (FSI) in the $(e, e' p)$ reaction in the limit of high Q^2 because the small-size $3q$ ejectile state formed after absorption of the virtual photon will weakly interact with the spectator nucleons. As a consequence, at high Q^2 the nuclear transparency T_A defined as a ratio of the experimentally measured cross-section to the theoretical cross section calculated in the plane-wave impulse approximation should tend to unity, and the experi-

mental missing-momentum distribution be close to the single-particle momentum distribution of the proton in the target nucleus. The observation of this effect, which is usually referred to as the color transparency (CT) phenomenon, would be a direct test of the space-time picture of hard processes predicted by perturbative QCD.

An accurate analysis of the FSI effects requires a quantum mechanical treatment of the evolution of the $3q$ ejectile wave function in the nuclear medium. At large Q^2 ($\geq 2 \text{ GeV}^2$), the kinetic energy of the struck proton $T_{\text{kin}} \approx Q^2/2m_p$ (here m_p is the proton mass) becomes large enough for the Glauber–Gribov coupled-channel multiple-scattering theory (CCMST)^{4,5} to be applicable for this purpose. The CCMST allows one to sum the quantum-mechanical amplitudes contributing to electroexcitation and diffractive deexcitation of the struck proton $p \rightarrow i_1 \rightarrow \dots \rightarrow i_\nu \rightarrow p$, provided that the nucleus wave function, $3q$ -nucleon scattering matrix, and

initial ejectile $3q$ wave function are known. In the CCMST the CT phenomenon corresponds to a cancellation between the rescattering amplitudes with elastic (diagonal) and inelastic (off-diagonal) intermediate states. Such a nontrivial cancellation becomes possible in QCD due to the existence of the CT sum rules,⁶ which relate diagonal and off-diagonal transition amplitudes.

Several studies were devoted to the study of CT effects in $(e, e'p)$ scattering within the coupled-channel formalism under different assumptions for the $3q$ -nucleon scattering amplitudes.⁶⁻¹⁰ The results of these analyses show that in the case of the integrated nuclear transparency the effect of the off-diagonal rescatterings is still small at $Q^2 \lesssim 10$ GeV². More recent calculations^{11,12} using the Green's function approach developed in Refs. 13, 14 also yield slow onset of CT. This prediction is consistent with the weak Q^2 -dependence of the nuclear transparency observed in the NE18 experiment.¹⁵

FSI effects vary with the missing-momentum \mathbf{p}_m and CT effects may be enhanced in some kinematical regions. The analyses of Refs. 8–10 show that the off-diagonal rescatterings give rise to forward–backward asymmetry of the missing-momentum distribution. In the forthcoming high-precision experiments at CEBAF, such a forward–backward asymmetry could have been a better signature of CT than the weak Q^2 -dependence of the integrated nuclear transparency. However, the nonzero Re/Im ratio, α_{pN} , for the forward pN scattering amplitude makes the nuclear medium dispersive for the struck proton and leads to a difference between its asymptotic momentum and the momentum inside the nucleus. This difference entails a longitudinal shift of the missing-momentum distribution and also generates the forward–backward asymmetry which has not been considered in Refs. 8–10. Within the context of the analysis of the inclusive data from SLAC, the role played by α_{pN} in eA scattering at high Q^2 has been pointed out in Ref. 16. Recent analysis^{17,18} demonstrated that the forward–backward asymmetry, associated with α_{pN} , at $Q^2 \lesssim 10$ GeV² is of the same order, or even larger than generated by the CT effects. Besides omitting the large effect of α_{pN} on the forward–backward asymmetry, CT effects in Refs. 8–10 were evaluated under certain qualitative approximations. In Ref. 9 the sum of the CCMST series was performed using the approximation of the effective-diffraction scattering matrix; Ref. 8 has used several unjustified approximations in the numerical calculations, and the authors of Ref. 10 have used incorrect initial ejectile $3q$ wave function (for the criticism to the approaches of Refs. 8, 10, see¹⁸). Furthermore, none of Refs. 8–10 has discussed the $p_{m\perp}$ -dependence of CT effects. On the whole, the theoretical understanding of the \mathbf{p}_m -dependence of CT effects is far from being complete, and further investigations of this problem are required.

In the present paper we study the missing-momentum dependence of the nuclear transparency in the region of $p_m \lesssim k_F$ (here $k_F \approx 250$ MeV/ c is the Fermi momentum). We perform an exact evaluation of the CCMST series, thus improving upon the approximation of the effective-diffraction matrix,⁹ and for the first time study the convergence of the CCMST expansion in the number of the excited proton

states. In our evaluation of CT effects we use the realistic pomeron part of the $3q$ -nucleon diffraction scattering matrix, which was previously used in Ref. 6 for calculation of the integrated nuclear transparency. We study the sensitivity of the results to the choice of the reggeon $3q$ -nucleon amplitudes.

The present analysis is focused on the use of the CCMST to describe the evolution of the $3q$ ejectile state during its propagation through the nuclear medium. We evaluate the CCMST series describing the nucleus wave function in the independent-particle shell model. The short-range correlations have been neglected, in view of the relatively small correlation effects on the SPMD¹⁹ and on the missing-momentum distribution in ${}^4\text{He}(p, 2p)$ found in the recent many-body Glauber analysis²⁰ at $p_m \lesssim k_F$. It is feasible that using Monte Carlo approaches for light nuclei and the local density approximation for heavier systems, one could eventually perform a more sophisticated analysis including short-range correlation.

The coupled-channel formalism is developed in a form which includes both the coherent and incoherent rescattering of the ejectile state in the nuclear medium. In the single-channel Glauber model, the role of the incoherent FSI was elucidated in Ref. 17. It was shown that in the shell model, allowance for both the coherent and incoherent rescattering corresponds to the inclusive $(e, e'p)$ reaction, when all the final states of the residual nucleus are involved, while the cross section obtained neglecting the incoherent rescattering is related to the exclusive $(e, e'p)$ reaction, when only the one-hole excitations of the target nucleus are allowed. The analysis¹⁷ shows that the incoherent rescatterings become important for $p_m \gtrsim 200$ – 250 MeV/ c . The impact of the incoherent off-diagonal rescattering on the onset of CT has not yet been treated quantitatively. We demonstrate that, in contact with the coherent off-diagonal rescattering, the contribution of the off-diagonal incoherent rescattering does not vanish at low Q^2 . We also show that in the case of incoherent rescattering the CT effects decrease the nuclear transparency.

The numerical calculations of the present paper are performed for the exclusive $(e, e'p)$ reaction. In the region of relatively small missing momenta ($p_m \lesssim 150$ – 200 MeV/ c), where the contribution of incoherent rescattering is negligible, our theoretical predictions may be compared with inclusive experimental data.

The correspondence between the coherent FSI and the one-hole excitations allows the \mathbf{p}_m -dependence of CT effects to be evaluated for different hole states. Because of the change of the spatial distribution of the bound proton, we find significant variations of nuclear transparency from the one hole state to another. We present estimates of CT effects for different acceptance windows in the transverse and longitudinal missing momentum. Previously, different hole excitations were considered²¹ in a model of the classical evolution of the ejectile state, which conflicts with the coherence properties of the CCMST.

The paper is organized as follows. In Sec. 2 we set out the CCMST formalism for the $(e, e'p)$ reaction. The emphasis is placed on the approximations which are necessary to

obtain the intuitive formula of the optical approximation. The considerations associated with the parametrization of the diffraction matrix and initial ejectile wave function are given in Sec. 3. In Sec. 4 we apply the formalism of the CCMST for qualitative analysis of the incoherent FSI. The numerical results obtained for exclusive $^{16}\text{O}(e, e'p)$ and $^{40}\text{Ca}(e, e'p)$ reactions are presented in Sec. 5. The summary and conclusions are presented in Sec. 6.

2. FSI IN THE GLAUBER–GRIBOV FORMALISM

We begin with the kinematics of quasielastic ($e, e'p$) scattering. In the present paper, following the usual practice,^{22–24} we assume that at high Q^2 the differential cross section of the ($e, e'p$) reaction may be expressed through the half off-shell ep -cross section σ_{ep} , and the distorted spectral function $S(E_m, \mathbf{p}_m)$ as

$$\frac{d\sigma}{dQ^2 d\nu dp d\Omega_p} = K \sigma_{ep} S(E_m, \mathbf{p}_m). \quad (1)$$

Here K is a kinematical factor, ν and \mathbf{q} are the (e, e') energy and momentum transfer, we define $Q^2 = \mathbf{q}^2 - \nu^2$, the struck proton has a momentum \mathbf{p} and energy $E(p) = T_{\text{kin}} + m_p$, the missing momentum and energy are defined as $\mathbf{p}_m = \mathbf{q} - \mathbf{p}$ and $E_m = \nu + m_p - E(p)$, and the z -axis is chosen along \mathbf{q} . Apart from E_m and \mathbf{p}_m the distorted spectral function depends on \mathbf{p} . In Eq. (1) and hereafter we suppress this variable. Equation (1) is written under the assumption that the difference between the spectral functions corresponding to absorption of the longitudinal (L) and transverse (T) photons, connected with the spin dependence of FSI and CT effects, can be neglected. We ignore the spin effects in FSI because when the energy of the struck proton is large they become small. As far as the CT effects are concerned, we will see that when the small-size $3q$ configurations dominate in hard ep scattering, which is of our interest in the present paper, the contributions of off-diagonal rescattering to the longitudinal and transverse spectral functions must be comparable. Since we do not distinguish between the longitudinal and transverse spectral functions, below we treat the electromagnetic current as a scalar operator. Also, note that Eq. (1) is for the cross section averaged over the azimuthal angle between the missing momentum and the (e, e') reaction plane, which does not contain the LT and TT interference response.²⁴

In terms of the distorted spectral function the nuclear transparency for a certain kinematical domain D of the missing energy and the missing momentum can be written as

$$T_A(D) = \frac{\int_D dE_m d^3 p_m S(E_m, \mathbf{p}_m)}{\int_D dE_m d^3 p_m S_{\text{PWIA}}(E_m, \mathbf{p}_m)}. \quad (2)$$

Here $S_{\text{PWIA}}(E_m, \mathbf{p}_m)$ is the theoretical spectral function of the plane-wave impulse approximation calculated without taking into account FSI. The missing-momentum distribution which is of our interest in the present paper is given by

$$w(\mathbf{p}_m) = \frac{1}{(2\pi)^3} \int dE_m S(E_m, \mathbf{p}_m). \quad (3)$$

The distorted spectral function can be written as

$$S(E_m, \mathbf{p}_m) = \sum_f |M_f(\mathbf{p}_m)|^2 \times \delta(E_m + E_{A-1}(\mathbf{p}_m) + m_p - m_A), \quad (4)$$

where $M_f(\mathbf{p}_m)$ is the reduced matrix element of the exclusive process $e + A_i \rightarrow e' + (A-1)_f + p$. Then, the missing-momentum distribution reads

$$w(\mathbf{p}_m) = \frac{1}{(2\pi)^3} \sum_f |M_f(\mathbf{p}_m)|^2. \quad (5)$$

In our analysis we confine ourselves to target nuclei with a large mass number, $A \gg 1$. Then, neglecting the center-of-mass correlations we can write $M_f(\mathbf{p}_m)$ as

$$M_f(\mathbf{p}_m) = \int d^3 r_1 \dots d^3 r_A \Psi_f^*(\mathbf{r}_2, \dots, \mathbf{r}_A) \times \Psi_i(\mathbf{r}_1, \dots, \mathbf{r}_A) S(\mathbf{r}_1, \dots, \mathbf{r}_A) \times \exp(i\mathbf{p}_m \cdot \mathbf{r}_1). \quad (6)$$

Here Ψ_i and Ψ_f are wave functions of the target and residual nucleus, respectively. The nucleon labelled '1' is chosen to be the struck proton. For brevity, in Eq. (6) and hereafter the spin and isospin variables are suppressed. The factor $S(\mathbf{r}_1, \dots, \mathbf{r}_A)$, which takes into account FSI of the ejectile state with spectator nucleons,

$$S(\mathbf{r}_1, \mathbf{r}_2, \dots, \mathbf{r}_A) = \frac{\langle p | \hat{S}_{3q}(\mathbf{r}_1, \mathbf{r}_2, \dots, \mathbf{r}_A) | E \rangle}{\langle p | E \rangle}, \quad (7)$$

where $|E\rangle$ is a three-quark wave function which describes the state of the proton after absorption of the virtual photon at point \mathbf{r}_1 and $\hat{S}_{3q}(\mathbf{r}_1, \mathbf{r}_2, \dots, \mathbf{r}_A)$ is an evolution operator of the three-quark system in the nuclear medium (as usual we assume that the spectator coordinates may be considered frozen during propagation of the fast $3q$ system through the nuclear medium). In the right-hand side of Eq. (7) the numerator is the probability amplitude for the $3q$ ejectile state escaping from the target nucleus $(A-1)_f$ debris to be observed in the proton state $|p\rangle$, and the denominator is the probability amplitude for the state $|E\rangle$ to be observed in the proton state as well. In terms of the electromagnetic current operator \hat{J}_{em} , the ejectile wave function is expressed as⁹

$$|E\rangle = \hat{J}_{em}(Q) |p\rangle = \sum_i |i\rangle \langle i | J_{em}(Q) | p \rangle = \sum_i G_{ip}(Q) |i\rangle, \quad (8)$$

where $G_{ip}(Q) = \langle i | J_{em}(Q) | p \rangle$ includes the electromagnetic formfactor of the proton as well as all transition formfactors for the electroexcitation of the proton $e + p \rightarrow e' + i$. It is worth noting that the ejectile wave function (8) is independent of the missing momentum and the \mathbf{p}_m -dependence of the reduced matrix element emerges only through the exponent $\exp(i\mathbf{p}_m \cdot \mathbf{r}_1)$ in the right-hand side of Eq. (6).

In the coupled-channel formalism the evolution operator of $3q$ system can be written in the following form:

$$\hat{S}_{3q}(\mathbf{r}_1, \dots, \mathbf{r}_A) = P_z \prod_{j=2}^A [1 - \theta(z_j - z_1) \times \hat{\Gamma}(\mathbf{b}_1 - \mathbf{b}_j, z_j - z_1)], \quad (9)$$

where \mathbf{b}_j and z_j are the transverse and longitudinal coordinates of the nucleons, and $\hat{\Gamma}(\mathbf{b}, z)$ is the operator profile function describing $3q$ -nucleon scattering. At high energy the $3q$ system propagates along the straight-path trajectory and can interact with the spectator nucleon j only for $z_j > z_1$, which is the origin of the z -ordering operator P_z and of the step-function $\theta(z_j - z_1)$ in Eq. (9). The matrix elements of the z -dependent operator profile function $\hat{\Gamma}(\mathbf{b}, z)$ can be written as

$$\langle i | \hat{\Gamma}(\mathbf{b}, z) | j \rangle = \exp(ik_{ij}z) \langle i | \hat{\Gamma}(\mathbf{b}) | j \rangle, \quad (10)$$

where $\hat{\Gamma}(\mathbf{b})$ is the usual operator profile function connected with the scattering matrix \hat{f} through the relation

$$\langle i | \hat{\Gamma}(\mathbf{b}) | j \rangle = -\frac{i}{8\pi^2} \int d^2q \exp(i\mathbf{q} \cdot \mathbf{b}) \langle i | \hat{f}(\mathbf{q}) | j \rangle \quad (11)$$

(the normalization of the scattering matrix is such that $\text{Im} \langle i | \hat{f}(\mathbf{q}=0) | i \rangle = \sigma_{\text{tot}}(iN)$), and k_{ij} is the longitudinal momentum transfer related to transition $iN \rightarrow jN^5$:

$$k_{ij} = \frac{m_i^2 - m_j^2}{2\varepsilon}, \quad (12)$$

here ε is the energy of the struck proton in the laboratory frame, m_i and m_j are the masses of the states $|i\rangle$ and $|j\rangle$. The exponent phase factor in Eq. (10) results from the additional phase which the $3q$ plane wave acquires after propagation the distance z . The whole phase factor, which the operator (9) yields in the case of the sequence of intermediate states $i_1 \rightarrow \dots \rightarrow i_\nu \rightarrow p$, is given by

$$F(i_1 \rightarrow \dots \rightarrow i_\nu \rightarrow p) = \exp \left[i \sum_{j=1}^{\nu} k_{p i_j} (z_j - z_{j-1}) \right], \quad (13)$$

where z_j ($j \geq 1$) is the longitudinal coordinate of the point where the transition $i_j N \rightarrow i_{j+1} N$ takes place, and z_0 corresponds to the transition $p + \gamma^* \rightarrow i_1$. It is easy to check, that the same phase factor (13) can be obtained by solving the set of the coupled-channel wave equations.

The sum over the final states of the residual nucleus in Eq. (5) can be performed with help of the closure relation

$$\sum_f \Psi_f(\mathbf{r}'_2, \dots, \mathbf{r}'_A) \Psi_f^*(\mathbf{r}_2, \dots, \mathbf{r}_A) = \prod_{j=2}^A \delta(\mathbf{r}_j - \mathbf{r}'_j). \quad (14)$$

After making use of (6), (14), the missing-momentum distribution (5) can be cast in the form

$$w(\mathbf{p}_m) = \frac{1}{(2\pi)^3} \int d^3r_1 d^3r'_1 \rho_D(\mathbf{r}_1, \mathbf{r}'_1) \exp[i\mathbf{p}_m(\mathbf{r}_1 - \mathbf{r}'_1)], \quad (15)$$

where

$$\rho_D(\mathbf{r}_1, \mathbf{r}'_1) = \int \prod_{j=2}^A d^3r_j \Psi_i(\mathbf{r}_1, \mathbf{r}_2, \dots, \mathbf{r}_A) \Psi_i^*(\mathbf{r}'_1, \mathbf{r}_2, \dots, \mathbf{r}_A) \times S(\mathbf{r}_1, \mathbf{r}_2, \dots, \mathbf{r}_A) S^*(\mathbf{r}'_1, \mathbf{r}_2, \dots, \mathbf{r}_A). \quad (16)$$

The function $\rho_D(\mathbf{r}_1, \mathbf{r}'_1)$ can be viewed as a FSI-modified one-body proton density matrix. In the plane-wave impulse approximation, when the FSI factors in the right-hand side of Eq. (16) equal unity, Eq. (16) reduces to the formula for usual one-body proton density matrix $\rho(\mathbf{r}_1, \mathbf{r}'_1)$, and Eq. (15) reduces to the expression for the single-particle momentum distribution

$$n_F(\mathbf{p}_m) = \frac{1}{(2\pi)^3} \int d^3r_1 d^3r'_1 \rho(\mathbf{r}_1, \mathbf{r}'_1) \times \exp[i\mathbf{p}_m(\mathbf{r}_1 - \mathbf{r}'_1)]. \quad (17)$$

As was stated in Sec. 1, we will describe the target nucleus in the independent-particle shell model. After we neglect the short-range correlations the A -body semidiagonal density matrix $\Psi_i(\mathbf{r}_1, \mathbf{r}_2, \dots, \mathbf{r}_A) \Psi_i^*(\mathbf{r}'_1, \mathbf{r}_2, \dots, \mathbf{r}_A)$ in Eq. (16) still contains the Fermi correlations. To carry out the integration over the coordinates of the spectator nucleons we neglect the Fermi correlations and replace the A -body semidiagonal density matrix by the factorized form

$$\Psi_i(\mathbf{r}_1, \mathbf{r}_2, \dots, \mathbf{r}_A) \Psi_i^*(\mathbf{r}'_1, \mathbf{r}_2, \dots, \mathbf{r}_A) \rightarrow \rho(\mathbf{r}_1, \mathbf{r}'_1) \prod_{i=2}^A \rho(\mathbf{r}_i). \quad (18)$$

Here

$$\rho(\mathbf{r}_1, \mathbf{r}'_1) = \frac{1}{Z} \sum_n \phi_n^*(\mathbf{r}'_1) \phi_n(\mathbf{r}_1)$$

is the proton shell model one-body density matrix and ϕ_n are the shell model wave functions, and $\rho_A(\mathbf{r})$ is the nucleon nuclear density normalized to unity. The errors connected with ignoring the Fermi correlations must be small because the ratio of the Fermi correlation length $l_F \sim 3/k_F$ to the interaction length corresponding to the interaction of the struck proton with the Fermi correlated spectator nucleons, $l_{int} \sim 4[\sigma_{\text{tot}}(pN)\langle n_A \rangle]^{-1}$ (here $\langle n_A \rangle$ is the average nucleon nuclear density), is a small quantity (~ 0.25). Recall that the factored approximation for the many-body nuclear density has been successfully employed, in connection with Glauber theory, in the analysis of a wealth of hadron-nucleus scattering data (for an extensive review on hA scattering see²⁵).

Making use of replacement (18) in Eq. (16) allows to write the missing-momentum distribution in the form

$$w(\mathbf{p}_m) = \frac{1}{(2\pi)^3} \int d^3r_1 d^3r'_1 \rho(\mathbf{r}_1, \mathbf{r}'_1) \Phi(\mathbf{r}_1, \mathbf{r}'_1) \times \exp[i\mathbf{p}_m(\mathbf{r}_1 - \mathbf{r}'_1)], \quad (19)$$

where the FSI factor $\Phi(\mathbf{r}_1, \mathbf{r}'_1)$ is given by

$$\Phi(\mathbf{r}_1, \mathbf{r}'_1) = \int \prod_{j=2}^A \rho_A(\mathbf{r}_j) d^3r_j \times S(\mathbf{r}_1, \mathbf{r}_2, \dots, \mathbf{r}_A) S^*(\mathbf{r}'_1, \mathbf{r}_2, \dots, \mathbf{r}_A). \quad (20)$$

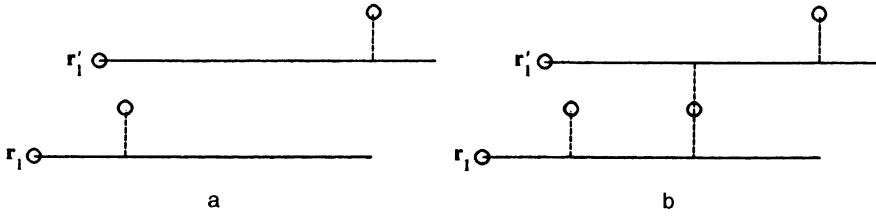


FIG. 1. Typical diagrams contributing to the operator $\hat{U}(\mathbf{r}_1, \mathbf{r}'_1)$ describing the evolution of the density matrix of the $3q$ ejectile state within the CCMST: (a) the diagram without the interaction between the two trajectories outgoing from \mathbf{r}_1 and \mathbf{r}'_1 , (b) the diagram containing the interaction between the trajectories generated by the $\hat{\Gamma}\hat{\Gamma}^*$ term in Eq. (23). The dotted lines attached to the straight-line trajectory originating from \mathbf{r}_1 or \mathbf{r}'_1 denote a profile function $\hat{\Gamma}(\mathbf{b}_j - \mathbf{b}_1, z_j - z_1)$ or $\hat{\Gamma}^*(\mathbf{b}_j - \mathbf{b}'_1, z_j - z'_1)$.

Substituting (7) into (20), we may write the FSI factor $\Phi(\mathbf{r}_1, \mathbf{r}'_1)$ in the following operator form:

$$\Phi(\mathbf{r}_1, \mathbf{r}'_1) = \langle pp | \hat{U}(\mathbf{r}_1, \mathbf{r}'_1) | ii' \rangle C_i C_i^*, \quad (21)$$

where

$$C_i = \frac{\langle i | E \rangle}{\langle p | E \rangle},$$

and the operator $\hat{U}(\mathbf{r}_1, \mathbf{r}'_1)$ is an evolution operator for the density matrix of the $3q$ system in the nuclear medium:

$$\hat{U}(\mathbf{r}_1, \mathbf{r}'_1) = \int \prod_{j=2}^A \rho_A(\mathbf{r}_j) d^3 r_j \hat{S}_{3q}(\mathbf{r}_1, \mathbf{r}_2, \dots, \mathbf{r}_A) \times \hat{S}_{3q}^*(\mathbf{r}'_1, \mathbf{r}_2, \dots, \mathbf{r}_A). \quad (22)$$

After substitution of the CCMST expression (9) for \hat{S}_{3q} into Eq. (22), it takes the form

$$\begin{aligned} \hat{U}(\mathbf{r}_1, \mathbf{r}'_1) = & \hat{P}_z \left[1 - \int_{z_1}^{\infty} dz \int d^2 b \hat{\Gamma}(\mathbf{b} - \mathbf{b}_1, z - z_1) \rho_A(\mathbf{b}, z) \right. \\ & - \int_{z'_1}^{\infty} dz \int d^2 b \hat{\Gamma}^*(\mathbf{b} - \mathbf{b}'_1, z - z'_1) \rho_A(\mathbf{b}, z) \\ & + \int_{\max(z_1, z'_1)}^{\infty} dz \int d^2 b \hat{\Gamma}(\mathbf{b} - \mathbf{b}_1, z - z_1) \\ & \left. \times \hat{\Gamma}^*(\mathbf{b} - \mathbf{b}'_1, z - z'_1) \rho_A(\mathbf{b}, z) \right]^{A-1}. \quad (23) \end{aligned}$$

We will refer to the first two terms in the square brackets on the right-hand side of Eq. (23) as $\hat{\Gamma}$ ($\hat{\Gamma}^*$) terms, and to the last one as the $\hat{\Gamma}\hat{\Gamma}^*$ term. The operator (23) can be graphically represented by the sum of the diagram as shown in Fig. 1. Every dotted line attached to the straight-line trajectory originating from the point \mathbf{r}_1 or \mathbf{r}'_1 denotes a profile function $\hat{\Gamma}(\mathbf{b}_j - \mathbf{b}_1, z_j - z_1)$ or $\hat{\Gamma}^*(\mathbf{b}_j - \mathbf{b}'_1, z_j - z'_1)$. The interaction between the two trajectories generated by the diagrams like that shown in Fig. 1b does not allow one to represent (23) in a factorized form in the coordinate and internal space of the two $3q$ systems propagating along the trajectories originating from \mathbf{r}_1 and \mathbf{r}'_1 .

The occurrence of the evolution operator for the $3q$ density matrix in Eq. (21) is not surprising since we evaluate the probability distribution for a subsystem ($3q$ ejectile state) for

the process involving a complex system ($3q$ ejectile state and residual nucleus). It is worth recalling that a similar interaction between the trajectories occurs also in the related problem of the passage of ultrarelativistic positronium through matter.²⁶

Equation (23) can further be simplified exploiting the fact that $\rho_A(\mathbf{b}, z)$ is a smooth function of the impact parameter \mathbf{b} as compared to the operator profile function. To leading order in the small parameter R_{3qN}^2/R_A^2 (R_{3qN} is a radius of $3q$ -nucleon interaction and R_A is the nucleus radius) we have

$$\int d^2 b \hat{\Gamma}(\mathbf{b} - \mathbf{b}_1, z - z_1) \rho_A(\mathbf{b}, z) \approx \frac{\hat{\sigma}(z)}{2} \rho_A(\mathbf{b}, z), \quad (24)$$

$$\begin{aligned} \int d^2 b \hat{\Gamma}(\mathbf{b} - \mathbf{b}_1, z - z_1) \hat{\Gamma}^*(\mathbf{b} - \mathbf{b}'_1, z - z'_1) \rho_A(\mathbf{b}, z) \\ \approx \hat{\eta}(\mathbf{b}_1 - \mathbf{b}'_1, z - z_1, z - z'_1) \rho_A\left(\frac{1}{2}(\mathbf{b}_1 + \mathbf{b}'_1), z\right), \quad (25) \end{aligned}$$

where

$$\hat{\sigma}(z) = 2 \int d^2 b \hat{\Gamma}(\mathbf{b}, z), \quad (26)$$

$$\hat{\eta}(\mathbf{b}, z, z') = \int d^2 \Delta \hat{\Gamma}(\mathbf{b} - \Delta, z) \hat{\Gamma}^*(\Delta, z'). \quad (27)$$

In terms of the diffraction scattering matrix \hat{f} the matrix elements of z -dependent operators (26) and (27) are given by

$$\langle i | \hat{\sigma}(z) | k \rangle = -i \exp(ik_{ij}z) \langle i | \hat{f}(\mathbf{q}=0) | k \rangle, \quad (28)$$

$$\begin{aligned} \langle ii' | \hat{\eta}(\mathbf{b}, z, z') | kk' \rangle \\ = \frac{\exp[i(k_{ik}z - k'_{i'k'}z')]}{16\pi^2} \int d^2 q \exp(i\mathbf{q}\mathbf{b}) \langle i | \hat{f}(\mathbf{q}) | k \rangle \\ \times \langle i' | \hat{f}(-\mathbf{q}) | k' \rangle^*. \quad (29) \end{aligned}$$

The results of the analysis of $(e, e'p)$ scattering within the Glauber model¹⁷ indicate that the variations of the missing-momentum distribution connected with the smearing corrections to the approximations (24) and (25) are $\leq 3\%$ at $p_m \leq 300$ MeV/c.

Making use of Eqs. 23–25 and exponentiating, which is a good approximation for $A \geq 10$, we finally get

$$\begin{aligned} \hat{U}(\mathbf{r}_1, \mathbf{r}'_1) = & \hat{P}_z \exp \left[-\frac{1}{2} \int_{z_1}^{\infty} dz \hat{\sigma}(z-z_1) n_A(\mathbf{b}_1, z) \right. \\ & -\frac{1}{2} \int_{z'_1}^{\infty} dz \hat{\sigma}^*(z-z'_1) n_A(\mathbf{b}'_1, z) \\ & + \int_{\max(z_1, z'_1)}^{\infty} dz \hat{\eta}(\mathbf{b}_1 - \mathbf{b}'_1, z-z_1, \\ & \left. \times z-z'_1) n_A \left(\frac{1}{2} (\mathbf{b}_1 + \mathbf{b}'_1), z \right) \right], \end{aligned} \quad (30)$$

where $n_A(\mathbf{r}) = A\rho_A(\mathbf{r})$ is the nucleon nuclear density.

As one can see from Eq. (27) the $\hat{\Gamma}\hat{\Gamma}^*$ term in Eqs. (23), (30) only becomes important for $|\mathbf{b}_1 - \mathbf{b}'_1| \lesssim R_{3qN} \sim 1$ fm. Such a short-range interaction between the two trajectories in the impact parameter plane must for the most part affect the missing-momentum distribution at $p_m \gtrsim 1/R_{3qN} \sim 200$ MeV/c. This fact becomes evident if one rewrites Eq. (19) in the convolution form

$$w(\mathbf{p}_m) = \frac{1}{(2\pi)^6} \int d^3R \int d^3k W_\rho(\mathbf{R}, \mathbf{p}_m - \mathbf{k}) W_\Phi(\mathbf{R}, \mathbf{k}), \quad (31)$$

where

$$W_\rho(\mathbf{R}, \mathbf{k}) = \int d^3r \rho \left(\mathbf{R} + \frac{\mathbf{r}}{2}, \mathbf{R} - \frac{\mathbf{r}}{2} \right) \exp(i\mathbf{k}\mathbf{r}) \quad (32)$$

is the familiar Wigner function, and

$$W_\Phi(\mathbf{R}, \mathbf{k}) = \int d^3r \Phi \left(\mathbf{R} + \frac{\mathbf{r}}{2}, \mathbf{R} - \frac{\mathbf{r}}{2} \right) \exp(i\mathbf{k}\mathbf{r}). \quad (33)$$

The representation (31) makes it clear that the short-range interaction between the two trajectories generated by the $\hat{\Gamma}\hat{\Gamma}^*$ term, which converts after Fourier transform (33) into the slowly decreasing tails of $W_\Phi(\mathbf{R}, \mathbf{k})$, will reveal itself for the most part at large missing momenta. Remarkably, although the operator $\hat{\eta}(\mathbf{b}, z, z')$ defined by Eq. (27) has short-range behavior only in the impact-parameter plane, the $\hat{\Gamma}\hat{\Gamma}^*$ term in Eq. (30) generates slowly decreasing tails of $W_\Phi(\mathbf{R}, \mathbf{k})$ in the longitudinal momenta as well. The formal origin of this effect is the nonanalytical behavior at $z_1 = z'_1$ of the function $\max(z_1, z'_1) = (z_1 + z'_1 + |z_1 - z'_1|)/2$, which is the lower limit of integration over z in the $\hat{\Gamma}\hat{\Gamma}^*$ term in Eq. (30). Such a nonanalytical function derives from the absence of an incoming proton plane wave, which is the real physical reason why the $\hat{\Gamma}\hat{\Gamma}^*$ term affects the longitudinal missing-momentum distribution (for the detailed quantum-mechanical analysis of this phenomenon see Ref. 17).

In the Glauber analysis of $(e, e'p)$ scattering¹⁷ it was shown that the $\hat{\Gamma}\hat{\Gamma}^*$ -generated effects correspond to incoherent rescattering of the struck proton in the nuclear medium, while the $\hat{\Gamma}(\hat{\Gamma}^*)$ terms describe FSI related to coherent rescattering. From the point of view of the shell model, the theoretical predictions obtained without taking into account the $\hat{\Gamma}\hat{\Gamma}^*$ term correspond to exclusive $(e, e'p)$ scattering, when only the one-hole excitations of the target nucleus are allowed, while the whole FSI factor including the $\hat{\Gamma}\hat{\Gamma}^*$ term corresponds to the inclusive process, when all the final states

of the residual nucleus are included.¹⁷ The results of Ref. 17 show that the $\hat{\Gamma}\hat{\Gamma}^*$ term increases the missing-momentum distribution by 3–7% at $|\mathbf{p}_m| \lesssim 250$ MeV/c in the parallel kinematics. For the transverse kinematics the same estimate is valid for $p_{m\perp} \lesssim 200$ MeV/c. The $\hat{\Gamma}\hat{\Gamma}^*$ term becomes especially important in the region $p_{m\perp} \gtrsim 250$ MeV/c, where it dominates in the missing-momentum distribution. Evidently, approximately the same situation will take place in CCMST when CT sets in.

The theoretical study of the CT effects including the $\hat{\Gamma}\hat{\Gamma}^*$ term in the region of large transverse missing momenta would be of great interest because in this case the missing-momentum distribution probes the $3q$ -nucleon scattering amplitude when the $3q$ wave function is still close to the initial ejectile wave function. Unfortunately, the calculations including the $\hat{\Gamma}\hat{\Gamma}^*$ term require the information about $3q$ -nucleon diffraction scattering matrix at arbitrary momentum transfer, as one can see from Eq. (29). It renders difficult an accurate estimate of the CT effects for the inclusive $(e, e'p)$ reaction in the region of large p_m . Still, even a qualitative understanding of the role of the $\hat{\Gamma}\hat{\Gamma}^*$ term is interesting and we comment on that in Sec. 4. We postpone a detail analysis of the inclusive reaction at large p_m for further publications.

In the present paper, we focus on the numerical calculations of the missing-momentum distribution for exclusive $(e, e'p)$ reaction, when the FSI is exhausted by the coherent rescattering. The corresponding FSI factor (we label it as Φ_{coh}), which may be obtained from Eq. (20) after neglecting the $\hat{\Gamma}\hat{\Gamma}^*$ term in the evolution operator (30), has the following factorized form

$$\Phi_{\text{coh}}(\mathbf{r}_1, \mathbf{r}'_1) = S_{\text{coh}}(\mathbf{r}_1) S_{\text{coh}}(\mathbf{r}'_1)^*, \quad (34)$$

where

$$\begin{aligned} S_{\text{coh}}(\mathbf{r}_1) = & \langle p | \hat{P}_z \exp \left[-\frac{1}{2} \int_{z_1}^{\infty} dz \hat{\sigma}(z) \right. \\ & \left. - z_1) n_A(\mathbf{b}_1, z) \right] | i \rangle C_i. \end{aligned} \quad (35)$$

Substituting (34) into (19), we arrive at the following expression for the missing-momentum distribution:

$$w(\mathbf{p}_m) = \frac{1}{Z} \sum_n \left| \int d^3r \phi_n(\mathbf{r}) \exp(i\mathbf{p}_m\mathbf{r}) S_{\text{coh}}(\mathbf{r}) \right|^2. \quad (36)$$

Equation (36) can also be obtained directly from Eqs. (5) and (6) if one includes in the sum over the final states of the residual nucleus in Eq. (5) only the one-hole excitations and neglects the Fermi correlations between the spectator nucleons. For the related intuitive optical potential consideration see Refs. 7, 8, and 10.

From the point of view of numerical calculations, it is convenient to evaluate $S_{\text{coh}}(\mathbf{r})$ treating in Eq. (35) the nondiagonal part of matrix $\hat{\sigma}(z-z_1)$ as a perturbation. Then, the FSI factor (35) can be expanded in a ν -fold off-diagonal rescattering series:

$$S_{\text{coh}}(\mathbf{r}) = \sum_{\nu=0}^{\infty} S_{\text{coh}}^{(\nu)}(\mathbf{r}), \quad (37)$$

where

$$S_{\text{coh}}^{(0)}(\mathbf{r}) = \exp\left[-\frac{1}{2} t(\mathbf{b}, \infty, z) \sigma_{pp}\right], \quad (38)$$

and

$$\begin{aligned} S_{\text{coh}}^{(\nu)}(\mathbf{b}, z) = & \left(-\frac{1}{2}\right)^\nu \sum_{i_1, \dots, i_\nu} \sigma'_{pi_\nu} \sigma'_{i_\nu i_{\nu-1}} \cdots \sigma'_{i_2 i_1} \frac{\langle i_1 | E \rangle}{\langle p | E \rangle} \\ & \times \exp(ik_{i_1 p} z) \int_z^\infty dz_1 n_A(\mathbf{b}, z_1) \\ & \times \exp\left[ik_{i_2 i_1} z_1 - \frac{1}{2} t(\mathbf{b}, z_1, z) \sigma_{i_1 i_1}\right] \\ & \times \int_{z_1}^\infty dz_2 n_A(\mathbf{b}, z_2) \exp\left[ik_{i_3 i_2} z_2 \right. \\ & \left. - \frac{1}{2} t(\mathbf{b}, z_2, z_1) \sigma_{i_2 i_2}\right] \cdots \int_{z_{\nu-1}}^\infty dz_\nu n_A(\mathbf{b}, z_\nu) \\ & \times \exp\left[ik_{pi_\nu} z_\nu - \frac{1}{2} t(\mathbf{b}, \infty, z_\nu) \sigma_{pp}\right], \quad \nu \geq 1. \quad (39) \end{aligned}$$

Here $\mathbf{r}=(\mathbf{b}, z)$, $\sigma'_{ik} = \sigma_{ik} - \delta_{ik} \sigma_{ii}$, the matrix $\hat{\sigma}$ is connected with the forward-diffraction scattering matrix $\hat{f}(\mathbf{q}=0)=i\hat{\sigma}$, and $t(\mathbf{b}, z_2, z_1) = \int_{z_1}^{z_2} dz n_A(\mathbf{b}, z)$ is the partial optical thickness. The zeroth-order term $S^{(0)}(\mathbf{r})$ in Eq. (37) describes the conventional Glauber result, while the terms with $\nu \geq 1$ correspond to the inelastic intermediate states contributing to electroexcitation and diffractive de-excitation of the proton $p \rightarrow i_1 \rightarrow \dots \rightarrow i_\nu \rightarrow p$. It precisely matches the oscillating exponential phase factors in Eq. (39), which leads to suppression of the contributions of the inelastic intermediate states at low energies of the struck proton. They are also the origin of the longitudinal asymmetry of the nuclear transparency produced by the off-diagonal rescattering. The emergence of these oscillating factors is a purely quantum-mechanical effect. In the classical treatment of FSI in terms of z -dependent $3q$ -nucleon cross section of Ref. 21 it is lacking and the longitudinal asymmetry of the missing-momentum distribution vanishes.

Equations (36)–(39) form a basis for evaluating the missing-momentum distribution within the CCMST for the exclusive $(e, e' p)$ reaction. For $p_m \lesssim 150\text{--}200$ MeV/ c , where the effect of the incoherent rescattering becomes small, our predictions can be compared directly with experimental data obtained without restrictions on the final states of the residual nucleus.

3. PARAMETRIZATION OF THE DIFFRACTION MATRIX AND THE INITIAL-EJECTILE WAVE FUNCTION

To proceed further with the numerical calculation of nuclear transparency, we need the diffraction matrix describing $3q$ -nucleon scattering and initial-ejectile wave function. At GeV energies of the struck proton, which are of interest in the present paper, the major contribution to the imaginary part of the amplitude $f(kN \rightarrow iN)$ comes from the pomeron exchange. Namely, this component of the $3q$ -nucleon scat-

tering matrix is for important mainly from the point of view of CT. Following Ref. 6, we construct the pomeron component of $\hat{\sigma}$ using the oscillator quark–diquark model of the proton:

$$\begin{aligned} \text{Im } f_p(kN \rightarrow iN) = & \text{Re } \sigma_{ik}^P \\ = & \int dz d^2 \rho \Psi_i^*(\boldsymbol{\rho}, z) \sigma(\rho) \Psi_k(\boldsymbol{\rho}, z), \quad (40) \end{aligned}$$

where $\Psi_{i,k}(\boldsymbol{\rho}, z)$ are the oscillator wave functions describing the quark–diquark states and $\sigma(\rho)$ is the dipole cross section describing the interaction of the quark–diquark system with a nucleon. For the oscillator frequency of the quark–diquark system we use the value $\omega_{qD}=0.35$ GeV, which yields a realistic mass spectrum of the proton excitations. As in Ref. 6, we take the dipole cross section in the form

$$\sigma(\rho) = \sigma_0 \left[1 - \exp\left(-\frac{\rho^2}{R_0^2}\right) \right]. \quad (41)$$

Equation (41) is motivated by the results of the calculation of the $q\bar{q}$ dipole cross section in the double gluon exchange model of the pomeron.²⁷ The parametrization (41) with $\sigma_0 \approx 50\text{--}60$ mb and $R_0 \approx 1.2\text{--}1.4$ fm allows one to describe both the CT effects in the quasi-elastic charge-exchange reaction $\pi^- A \rightarrow \pi^0 A'$ ²⁸ and the nuclear shadowing and diffraction cross section in deep inelastic scattering.^{29,30} The $q\bar{q}$ dipole cross section extracted from the experimental data on vector meson electroproduction³¹ also appears to be close to one used in Refs. 28–30. Of course, due to the nonzero diquark size, the parameters of the quark–diquark dipole cross section in Eq. (11) may differ from the ones obtained from the analysis of the meson exchange process and deep inelastic scattering. Following Ref. 6, we set $\sigma_0=80$ mb and adjust R_0 to reproduce $\sigma_{\text{tot}}^{\text{exp}}(pN)$. For a realistic evaluation of the onset of CT, it is important for the model diffraction matrix to reproduce the gross features of diffractive pN scattering in the resonance region. Our diffraction matrix obtained with the above set of parameters yields the value of the ratio between the diffractive and elastic pN cross sections $\sigma_{\text{diff}}(pp)/\sigma_{\text{el}}(pp) \approx 0.25$, which is in agreement with the experimental data.³² Moreover, we obtain a good description of the diffractive mass spectrum observed in pN scattering.³³

The real parts of the diagonal $f(iN \rightarrow iN)$ for $i \neq p$, and off-diagonal $f(iN \rightarrow kN)$ amplitudes are not known experimentally. At GeV energies of the struck proton, they are connected with the reggeon exchanges. In contrast to the pomeron exchange at present we do not have a reliable theoretical model for the reggeon contribution to the $3q$ -nucleon amplitude even for a small-size $3q$ system. As a reference value, we consider the choice $\alpha_1=1, \alpha_2=0$ in the parametrizations

$$\begin{aligned} \text{Re } f_R(iN \rightarrow iN) = & \alpha_1 \text{Re } f_R(pN \rightarrow pN) \\ = & \frac{\alpha_1}{2} [\alpha_{pp} \sigma_{\text{tot}}(pp) + \alpha_{pn} \sigma_{\text{tot}}(pn)], \\ \text{Re } f_R(iN \rightarrow kN) = & \alpha_2 \text{Im } f_p(iN \rightarrow kN), \quad i \neq k. \quad (42) \end{aligned}$$

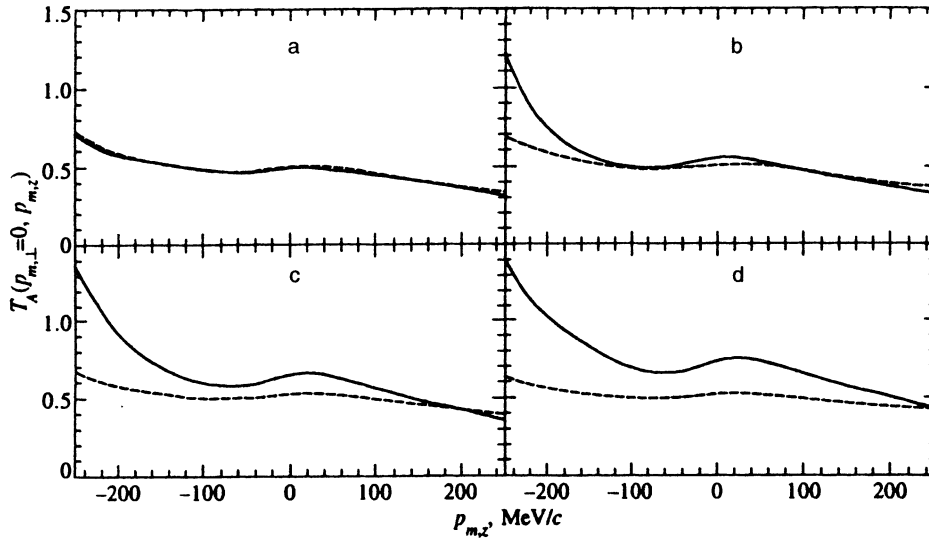


FIG. 2. Nuclear transparency in exclusive $^{16}\text{O}(e, e'p)$ scattering in parallel kinematics, $p_{m,\perp}=0$, calculated within CC-MST (solid curves) and in the Glauber model (dashed curves) for (a) $Q^2=5$ GeV^2 , (b) $Q^2=10$ GeV^2 , (c) $Q^2=20$ GeV^2 , and (d) $Q^2=40$ GeV^2 .

Even though the above choice of $\alpha_{1,2}$ can be justified within the framework of the dual parton model,³⁴ we are fully aware that it should only be regarded as an estimate, and will study the sensitivity of the results to the values $\alpha_{1,2}$.

Besides the matrix $\hat{\sigma}$, the evaluation of $w(\mathbf{p}_m)$ requires the ejectile wave function $|E\rangle$. In the present paper we optimize for CT effects, assuming the dominance of the small-size $3q$ configurations in the matrix elements $\langle i|J_{em}(Q)|p\rangle$ for the resonant states with masses in the GeV region.¹ This amounts to a strong assumption that the probability amplitude for the ejectile state to be observed in state $|i\rangle$,

$$\langle i|E\rangle = \langle i|J_{em}(Q)|p\rangle \propto \phi_i^* \left(\rho \sim \frac{1}{Q} \right), \quad (43)$$

where ϕ_i is the coordinate wave function of the state $|i\rangle$. By virtue of Eq. (43), the initial-ejectile wave function can be chosen in a point-like form. We parametrize it in the form $\langle p|E\rangle \propto \exp(-C\rho^2 Q^2)$ with $C=1$. We would like to emphasize that the possibility of using the point-like initial-ejectile

wave function for the study of CT effects by no means implies that the real ejectile state $|E\rangle$ actually has a size $\sim 1/Q$. On the contrary, it is evident that the ejectile state formed after absorption of the virtual photon has exactly the same transverse size as the proton.³⁵ The solution to this puzzling situation is obvious. Equation (43) is only valid for electroproduction of the proton and its low-mass excitations, which requires the hard-gluon exchanges between the quarks of the $3q$ system. The electroproduction of the high-mass states with masses $\sim |q|$ does not require such exchanges, and Eq. (43) does not hold in this case. However, the off-diagonal rescattering including the heavy intermediate states is suppressed. This is due first to the oscillating factors in Eq. (39): only the states which satisfy the coherency constraint $m_i^2 - m_p^2 \lesssim Q^2/R_A m_p$ can contribute to FSI. Second, the off-diagonal diffraction amplitudes $f(iN \rightarrow jN)$ also become small when the masses m_i and m_j differ strongly.

The above suppression of the heavy intermediate states makes the theoretical predictions insensitive to the specific

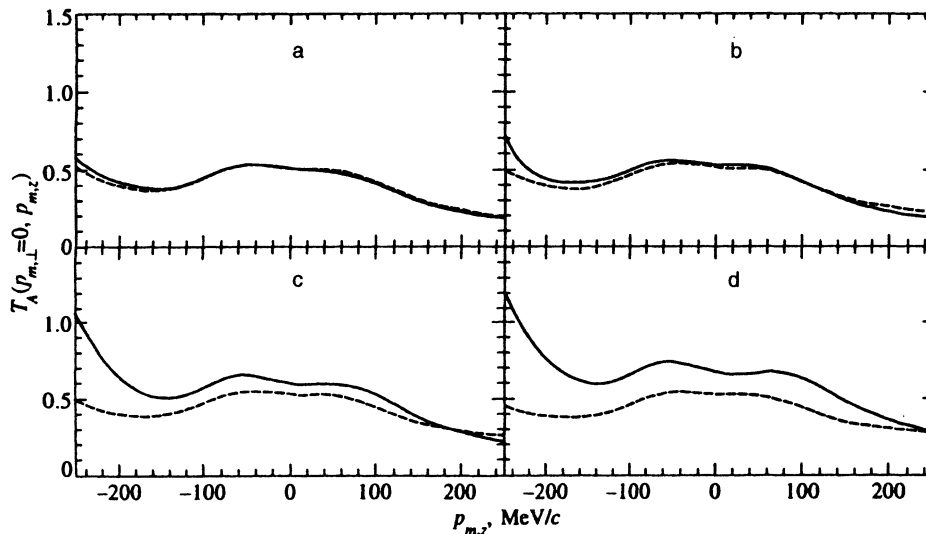


FIG. 3. The same as Fig. 2, but for $^{40}\text{Ca}(e, e'p)$ scattering.

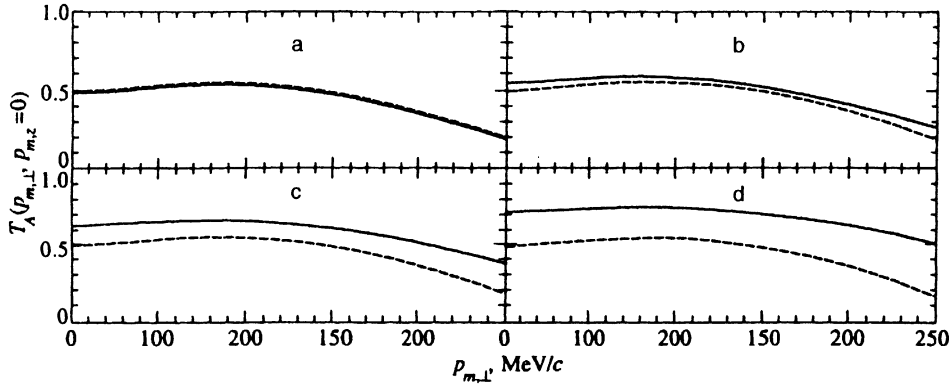


FIG. 4. Nuclear transparency in exclusive $^{16}\text{O}(e, e'p)$ scattering in transverse kinematics, $p_{m,z}=0$, calculated within the CCMST (solid curves) and in the Glauber model (dashed curves). The notations are the same as in Fig. 2.

form of the point-like initial-ejectile wave function. For instance, for the Gaussian parametrization used in the present paper the missing-momentum distribution must be insensitive to the value of C as long as $C \geq 1/Q^2 \rho_0^2$ holds, ρ_0 denotes the position of the first node in the wave functions of the excited states satisfying the coherency requirement. We checked that in the region $Q^2 \leq 40 \text{ GeV}^2$, which we discuss in the present paper, our numerical results are practically independent of the parameter C for $C \geq 0.1$. It is worth noting that the weak sensitivity of CT effects to the specific choice of the point-like initial-ejectile wave function also vindicates neglecting the difference between the CT effects for the longitudinal and transverse spectral functions.

To conclude this section one remark on the nonrelativistic description of the $3q$ system is in order. Of course, the nonrelativistic approach cannot be justified for the high excited states. However, our numerical results show that due to the coherency constraint the dominant role in the regime of the onset of CT plays the first excitation of the proton. This, in part, vindicates the use of the nonrelativistic model. Still, we regard the nonrelativistic quark-diquark model only as a basis which allows us to obtain a realistic diffraction scattering matrix, which is truly important from the point of view of the CCMST.

4. QUALITATIVE ANALYSIS OF THE INCOHERENT FSI

As was shown in Sec. 2, an evaluation of the missing-momentum distribution with the $\hat{\Gamma}\hat{\Gamma}^*$ term included requires information on the $3q$ -nucleon scattering matrix at arbitrary

momentum transfer. Despite the ensuing model-dependence of an analysis of the inclusive $(e, e'p)$ reaction, certain conclusions on the role of the incoherent rescattering can be reached without specifying the explicit form of the scattering matrix. Here we consider the simpler case of the integrated nuclear transparency. For the inclusive $(e, e'p)$ reaction we can write

$$T_A^{\text{inc}} = T_A^{\text{exc}} + \Delta T_A, \quad (44)$$

where

$$T_A^{\text{exc}} = \int d^3r \rho_A(\mathbf{r}) \Phi_{\text{coh}}(\mathbf{r}, \mathbf{r}) \quad (45)$$

is the transparency for exclusive $(e, e'p)$ scattering when only the coherent rescattering is allowed, and the contribution of the incoherent FSI is given by

$$\Delta T_A = \int d^3r \rho_A(\mathbf{r}) [\Phi(\mathbf{r}, \mathbf{r}) - \Phi_{\text{coh}}(\mathbf{r}, \mathbf{r})]. \quad (46)$$

To simplify the problem, let us consider the two-channel model, which involves only one resonance state $|p^*\rangle$. We estimate ΔT_A expanding the evolution operator (30) up to first order in the $\hat{\Gamma}\hat{\Gamma}^*$ term. Notice that the one-fold incoherent rescattering practically saturates the missing-momentum distribution in the region of $p_m \leq 300 \text{ MeV}/c$, which gives the dominant contribution to T_A^{inc} .¹⁷ Also, we neglect the off-diagonal coherent rescatterings. Then, making use of Eqs. (21), (30), (34), and (46) after some simple algebra we get

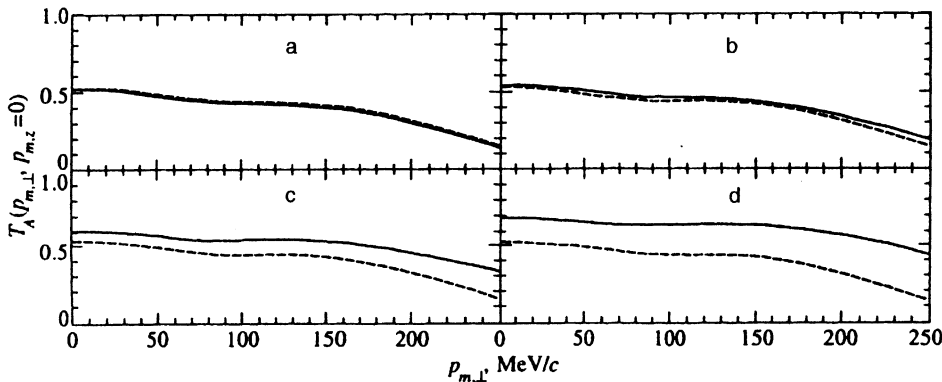


FIG. 5. The same as Fig. 4, but for $^{40}\text{Ca}(e, e'p)$ scattering.

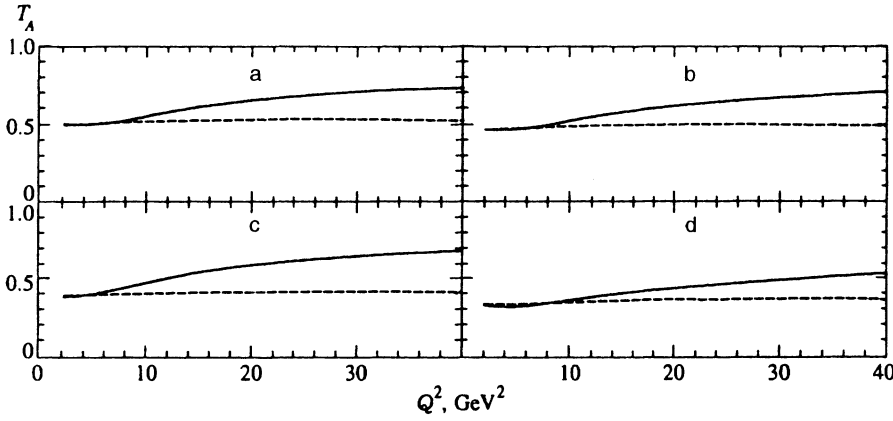


FIG. 6. The Q^2 -dependence of nuclear transparency for exclusive $^{16}\text{O}(e, e'p)$ scattering at different windows D in the transverse ($p_{m,\perp} \leq 200$ MeV/c) and longitudinal [(a) $|p_{m,z}| \leq 50$ MeV/c; (b) $|p_{m,z}| \leq 200$ MeV/c; (c) -200 MeV/c $\leq p_{m,z} \leq 0$; (d) $0 \leq p_{m,z} \leq 200$ MeV/c] missing momentum obtained within the CCMST (solid curves) and in the Glauber model (dashed curves).

$$\begin{aligned} \Delta T_A = & \frac{1}{16\pi^2} \int d^2q [|\langle p | \hat{f}(\mathbf{q}) | p \rangle|^2 I_{pp} \\ & + |\langle p | \hat{f}(\mathbf{q}) | p^* \rangle|^2 I_{p^*p^*} |C_{p^*}|^2 + 2 \text{Re} \langle p | \hat{f}(\mathbf{q}) | p^* \rangle \\ & \times \langle p | \hat{f}(\mathbf{q}) | p \rangle^* I_{p^*p} C_{p^*}]. \end{aligned} \quad (47)$$

Here

$$\begin{aligned} I_{pp} = & \int d^2b_1 dz_1 \rho_A(\mathbf{b}_1, z_1) \int_{z_1}^{\infty} dz n_A(\mathbf{b}_1, z) \\ & \times \exp[-\text{Re} \sigma_{pp} t(\mathbf{b}_1, \infty, z_1)], \end{aligned} \quad (48)$$

$$\begin{aligned} I_{p^*p^*} = & \int d^2b_1 dz_1 \rho_A(\mathbf{b}_1, z_1) \int_{z_1}^{\infty} dz n_A(\mathbf{b}_1, z) \\ & \times \exp[-\text{Re} \sigma_{pp} t(\mathbf{b}_1, \infty, z) - \text{Re} \sigma_{p^*p^*} t(\mathbf{b}_1, z, z_1)], \end{aligned} \quad (49)$$

$$\begin{aligned} I_{p^*p} = & \int d^2b_1 dz_1 \rho_A(\mathbf{b}_1, z_1) \int_{z_1}^{\infty} dz n_A(\mathbf{b}_1, z) \\ & \times \exp(ik_{pp^*} z) \exp\left[-\text{Re} \sigma_{pp} t(\mathbf{b}_1, \infty, z) \right. \\ & \left. - \frac{(\sigma_{p^*p^*} + \sigma_{pp}^*)}{2} t(\mathbf{b}_1, z, z_1)\right]. \end{aligned} \quad (50)$$

The diagonal and off-diagonal amplitudes in Eq. (47) are related through the CT sum rule

$$\langle p | \hat{f}(\mathbf{q}) | p \rangle + \langle p | \hat{f}(\mathbf{q}) | p^* \rangle C_{p^*} = 0. \quad (51)$$

Making use of (51), we can write (47) as

$$\Delta T_A = \sigma_{el}(pN) [I_{pp} + I_{p^*p^*} - 2 \text{Re} I_{p^*p}]. \quad (52)$$

At low energies of the struck proton, when $k_{pp^*} R_A \approx (m_{p^*}^2 - m_p^2) R_A / 2\varepsilon \gg 1$ holds, the p^*p interference term in Eq. (52) (the last term in the square brackets in the right-hand side of Eq. (52)) becomes small and we get

$$\Delta T_A \approx \sigma_{el}(pN) [I_{pp} + I_{p^*p^*}]. \quad (53)$$

At high energy, when $k_{pp^*} R_A \approx (m_{p^*}^2 - m_p^2) R_A / 2\varepsilon \ll 1$, the p^*p interference term in Eq. (52) is not suppressed and will in part cancel the contributions of the first two terms. Thus, we see that, in contrast to the coherent FSI, in the case of the incoherent FSI the CT effects decrease nuclear transparency. Hence, a ‘‘conspiracy’’ of the CT effects related to the coherent and incoherent rescattering must take place in the integrated nuclear transparency measured in inclusive $(e, e'p)$ reaction. According to the qualitative consideration of Sec. 2 and the analysis in,¹⁷ the contribution of the incoherent rescattering to the missing-momentum distribution for the most part comes from the region $p_{m\perp} \geq 200$ –250 MeV/c. Evidently, the difference between ΔT_A at low and high energies comes just from this region of the missing momentum.

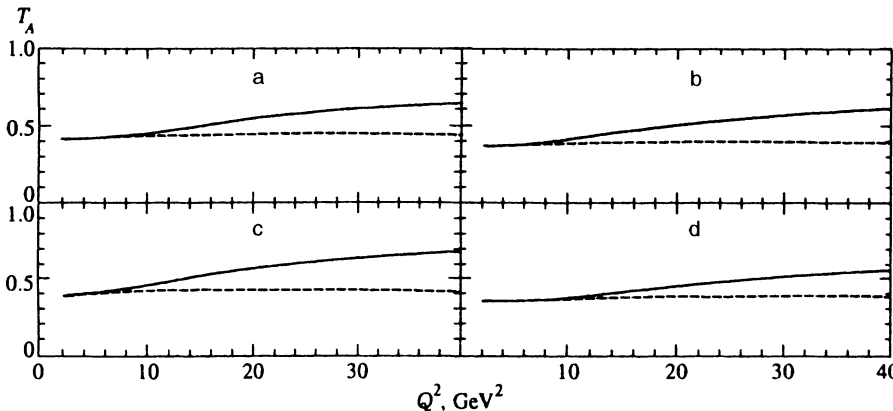


FIG. 7. The same as Fig. 6, but for $^{40}\text{Ca}(e, e'p)$ scattering.

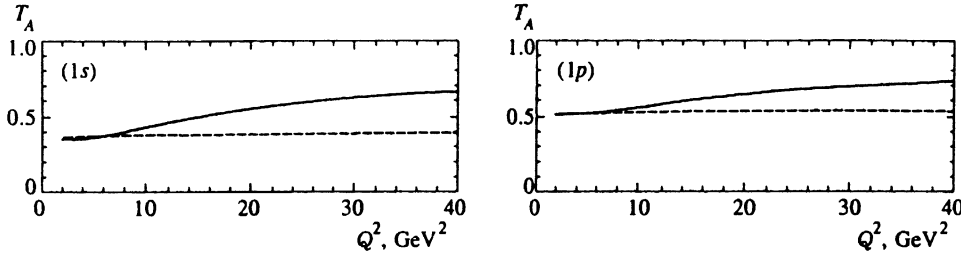


FIG. 8. The Q^2 -dependence of nuclear transparency for exclusive $^{16}\text{O}(e, e'p)$ scattering for excitations of the separate hole states at the kinematical window $p_{m\perp}, |p_{m,z}| < 200$ MeV/c obtained within the CCMST (solid curves) and in the Glauber model (dashed curves).

Hence it is advantageous to perform experimental measurements of the nuclear transparency separately in the regions of $p_{m\perp} \lesssim 200$ MeV/c and $p_{m\perp} \gtrsim 250$ MeV/c. At small momenta the CT signal is increasing the transparency, while at large momenta the CT will manifest itself through a decrease in the transparency.

Equation (53) demonstrates that, on the contrary to the wide-spread opinion, in inclusive $(e, e'p)$ reaction the contribution of the off-diagonal rescattering survives at low energies. To this effect, the inclusive $(e, e'p)$ scattering differs drastically from exclusive $(e, e'p)$ reaction or elastic hadron-nucleus scattering, where at low energies the predictions of the CCMST and the Glauber model are close to each other. Of course, one should bear in mind that Eq. (53) is obtained in the idealized quark model, which ignores the finite value of the resonance width Γ_{p^*} . Inclusion of the finite Γ_{p^*} will lead to a suppression of the second term in the right-hand side of Eq. (53) at sufficiently small energies $\varepsilon \lesssim \Gamma_{p^*} m_p l_{\text{int}} \sim 2$ GeV (here $l_{\text{int}} \sim (\sigma_{\text{tot}}(pN) \langle n_A \rangle)^{-1}$ is the average interaction length of the $3q$ system in the nuclear medium). However, it is important that the scale of the energy, where the finite-width effects become strong, are smaller by a factor ~ 3 – 5 than the energy scale of the CT effects $\varepsilon \sim (m_{p^*}^2 - m_p^2) R_A / 2$. It means that there is a certain energy interval in which the CT effects are still small, but, nonetheless, the Glauber model is not justified for evaluation of the contribution to the missing-momentum distribution of the incoherent rescattering.

It is appropriate here to comment on the previous analyses of the Q^2 -dependence of the integrated nuclear transparency. In Refs. 6–8 the calculations were performed making use of the optical potential form of the FSI factor. This means that the integrated transparency of Refs. 6–8 corresponds to the exclusive $(e, e'p)$ reaction. The authors of Refs. 11 and 12 also used the optical potential FSI factor. However, they replaced the total pN cross section by the inelastic pN cross section $\sigma_{in}(pN)$. In the Glauber model the integrated transparency in the inclusive $(e, e'p)$ scattering is indeed controlled by $\sigma_{in}(pN)$ (see the discussion of this problem in Ref. 17). The analysis of the present paper makes clear that the CT effects from the incoherent rescattering cannot be described by a simple renormalization of the diffraction scattering matrix in the equations obtained in the optical-potential approach. For this reason prescription of Refs. 11 and 12 is not justified.

It is worth noting that the above analysis indicates that in the case of the quasielastic $(p, 2p)$ scattering a complicated interplay of the CT effects from the coherent and incoherent

rescattering may also take place. Evidently, in this process too, the contribution of the off-diagonal incoherent rescattering will survive at low energies. In $(p, 2p)$ scattering, the contribution of the incoherent rescattering appears to be considerably enhanced in a comparison with $(e, e'p)$ reaction.³¹ For this reason an analysis of the CT effects in $(p, 2p)$ scattering must include the incoherent rescattering, which was neglected in all previous works on this problem.

5. NUMERICAL RESULTS FOR THE EXCLUSIVE $(e, e'p)$ SCATTERING

In this section we present our numerical results for the nuclear transparency in exclusive $(e, e'p)$ scattering obtained making use of Eqs. (36)–(39). We recall, that in the region $p_m \lesssim 150$ – 200 MeV/c, where the contribution of the incoherent rescattering becomes small, our theoretical predictions may be compared directly with experimental data for the inclusive $(e, e'p)$ reaction. The numerical calculations were carried out for the target nuclei ^{16}O and ^{40}Ca . In our calculations we used the harmonic oscillator shell wave functions. The oscillator shell model frequency ω_{osc} for the two nuclei were adjusted to reproduce the experimental value of the root-mean-square radius of the charge distribution $\sqrt{\langle r^2 \rangle}$. We used the values³⁶ $\sqrt{\langle r^2 \rangle} = 2.73$ fm for ^{16}O , and $\sqrt{\langle r^2 \rangle} = 3.47$ fm for ^{40}Ca , which correspond to an oscillator radius $r_{\text{osc}} = 1/\sqrt{m_p \omega_{\text{osc}}}$ equal to 1.74 fm for ^{16}O and 1.95 fm for ^{40}Ca . The difference between the charge distribution and the proton nuclear density connected with the proton charge radius was taken into account. We checked that our set of harmonic oscillator shell wave functions gives the charge density and the single-particle momentum distribution in the region of $p_m \lesssim 250$ – 300 MeV/c, which are practically indistinguishable from the results of more involved Hartree–Fock calculations. Notice that in this momentum region the single-particle momentum distribution calculated in the harmonic oscillator shell model is also close to the one obtained within a many-body approach with realistic nucleon–nucleon potential in Ref. 37. In our calculations we define the pN cross section and α_{pN} as mean values of these quantities for the pp and pn scatterings. We borrowed the experimental data on pp , pn cross sections and α_{pp} , α_{pn} from the recent review.³⁸

To illustrate the role of the off-diagonal rescatterings which are responsible for the CT effects, we present a systematic comparison of the results obtained within the CCMST and the ones obtained in the Glauber model. The number of the included resonance states and the off-diagonal

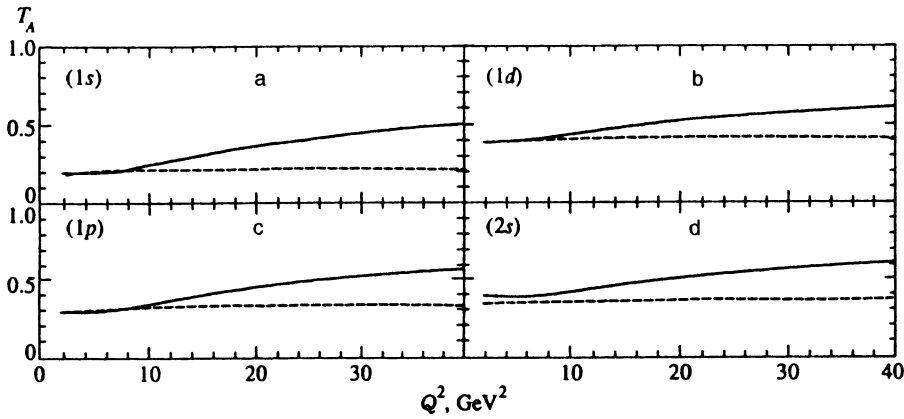


FIG. 9. The same as Fig. 8, but for $^{40}\text{Ca}(e, e'p)$ scattering.

rescatterings used in Eqs. (37)–(39) to obtain the curves corresponding to the CCMST were equal to 4 and 3, respectively. We checked that the contributions from higher excitations and rescatterings with $\nu > 3$ are negligible in the region of $Q^2 \leq 40 \text{ GeV}^2$ considered in the present paper.

In Figs. 2 and 3 we show the behavior of the nuclear transparency versus $p_{m,z}$ for the purely parallel kinematics for $Q^2 = 5, 10, 20,$ and 40 GeV^2 . Notice that the nuclear transparency evaluated even in the Glauber model without off-diagonal rescatterings has sizeable asymmetry about $p_{m,z} = 0$ connected with nonzero α_{pN} , which was neglected in previous works. Figures 2 and 3 demonstrate that the CT effect in the region of $Q^2 \leq 10 \text{ GeV}^2$ is still small at $|p_{m,z}| \leq 150 \text{ MeV}/c$. However, at $p_{m,z} \approx -250 \text{ MeV}/c$ it becomes sizeable and could be observed in a high-precision experiment. Our calculations show that the situation is more favorable in the case of light nucleus.

The results for nuclear transparency in the case of the transverse kinematics are presented in Figs. 4 and 5. We see that, as in the case of the parallel kinematics, the distortion effects are considerable even in the Glauber model. The CT effects are still small in the region of $Q^2 \leq 10 \text{ GeV}^2$. They

become important only at $Q^2 \geq 20 \text{ GeV}^2$, especially at large $p_{m,\perp}$.

In Figs. 6 and 7 we show our predictions for the integrated nuclear transparency. In order to demonstrate the dependence of the nuclear transparency on the choice of the kinematical domain D in the definition (2), we calculated T_A for four different windows in the missing momenta. One sees that the most steep rise of T_A takes place for the window containing negative values of the longitudinal missing momentum.

We also calculated the integrated nuclear transparency for the excitation of separate hole states in the target nucleus for the kinematical domain $p_{m,\perp}, |p_{m,z}| < 200 \text{ MeV}/c$. The results are presented in Figs. 8 and 9. These figures show that the CT effects are different for the different shell states, being larger for the $1s$ state. This fact is further illustrated by Figs. 10–13, which show the missing-momentum distribution for excitation of the separate hole states for the parallel and transverse kinematics at $Q^2 = 5$ and 40 GeV^2 . Unfortunately, however, the experimental information about deeply bound hole states is most difficult to extract since their strength is fragmented over a wide range of missing energy.

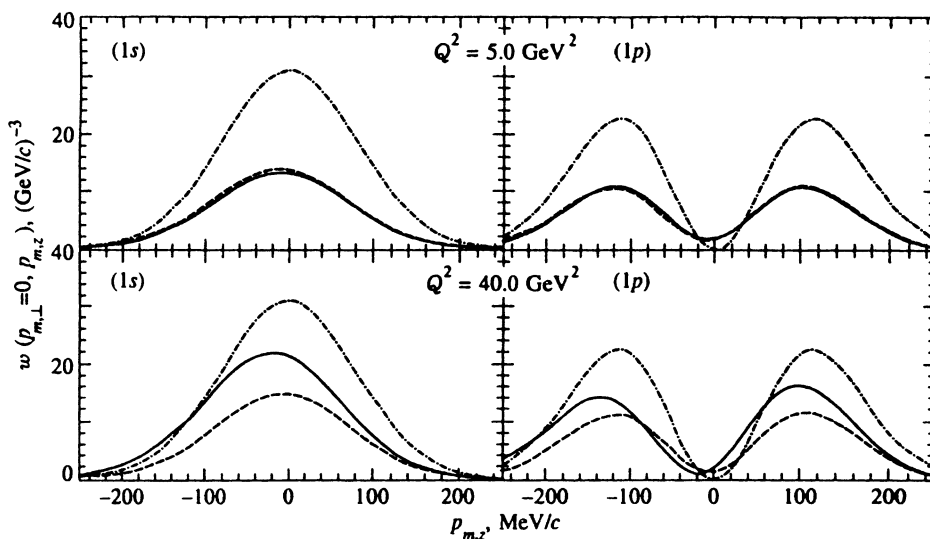


FIG. 10. The missing-momentum distribution for $^{16}\text{O}(e, e'p)$ scattering in parallel kinematics $p_{m,\perp} = 0$ for the separate shells calculated within the CCMST (solid curve) and in the Glauber model (dashed curve). The dot-and-dash curve shows the single-particle momentum distribution.

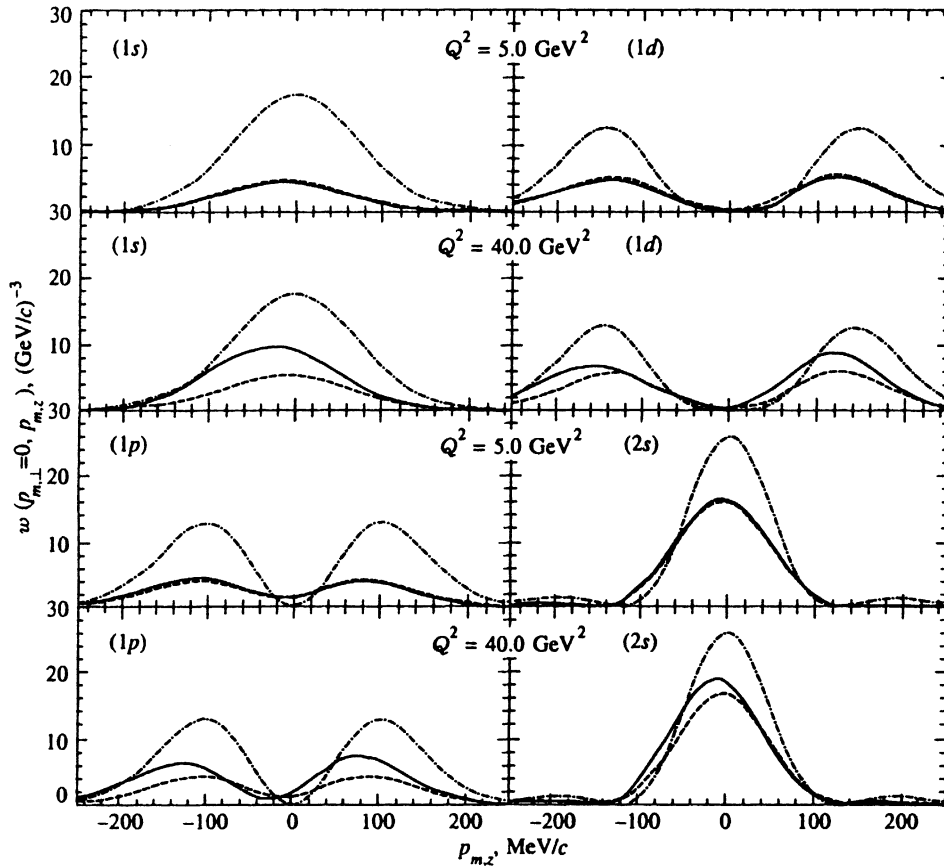


FIG. 11. The same as Fig. 10, but for $^{40}\text{Ca}(e, e'p)$ scattering.

The relative CT effect of different excitations of the $3q$ ejectile state is demonstrated in Fig. 14, where we plot the integrated nuclear transparency for the window $p_{m\perp}, |p_{mz}| < 200$ MeV/c calculated for the number of included intermediate states, $n=1,2,3,4$. We see that in the region $Q^2 \lesssim 40$ GeV 2 the FSI effects are practically saturated for $n=3$. For $Q^2 \lesssim 20$ GeV 2 in the CCMST formalism it is sufficient to take into account only the first excitation of the proton.

Our numerical results show that the experimental observation of the CT phenomenon at $Q^2 \lesssim 20$ GeV 2 is a delicate problem. For this reason it is important to understand how large the uncertainties of the theoretical predictions are for the contribution of the off-diagonal rescattering. The least reliable ingredient is the reggeon part of the $3q$ -nucleon amplitudes. To estimate the corresponding uncertainties we studied the sensitivity of the results to the choice of the reggeon parameters α_1 and α_2 in (42), which control the

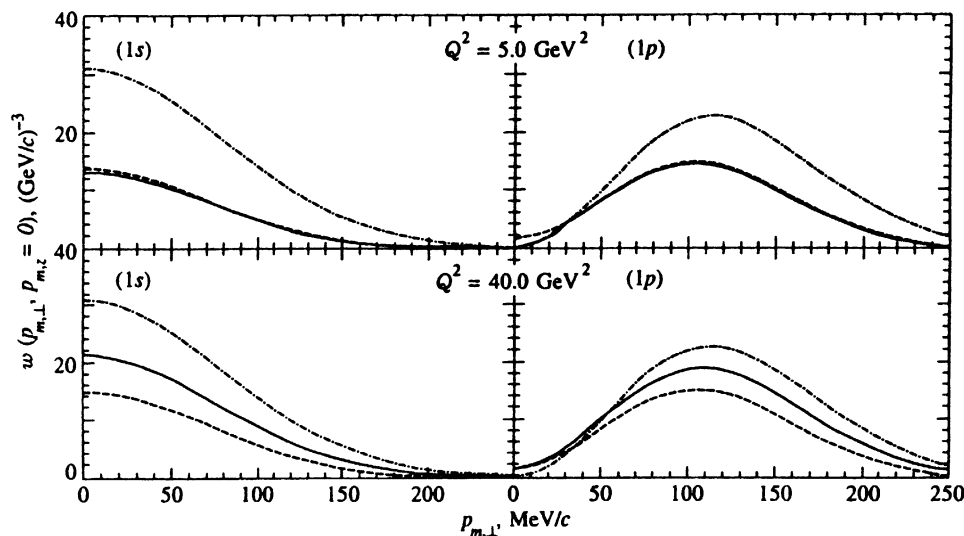


FIG. 12. The same as Fig. 10, but for transverse kinematics.

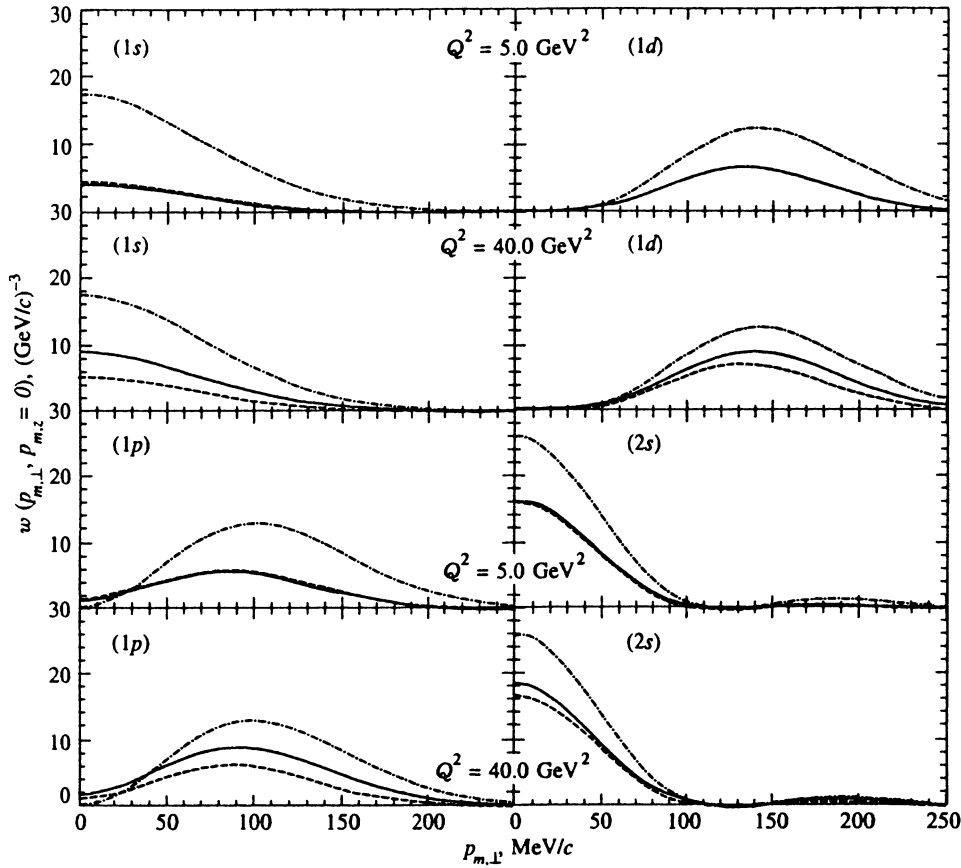


FIG. 13. The same as Fig. 11, but for transverse kinematics.

diagonal and off-diagonal matrix elements, respectively. Changing α_1 has practically no effect on the results. However, the dependence on α_2 is not negligible. The suppression of the off-diagonal $3q$ -nucleon amplitudes in comparison with the diagonal ones is expected to be stronger for the reggeon exchange than for the pomeron one. For this reason we chose for the upper bound of $|\alpha_2|$ the value 0.5, which is about the maximum value of $|\alpha_{pN}|$. The effect of variation of α_2 in the range $(-0.5, 0.5)$ for integrated nuclear transparency in the window $p_{m,\perp}, |p_{m,z}| < 200$ MeV/c is illustrated in Fig. 15. As one can see, the positive values of α_2 decrease the nuclear transparency, and can to a certain extent obscure the CT effects at $Q^2 \lesssim 20$ GeV². In Figs. 16 and 17 we demonstrate the effect of varying of α_2 for the unintegrated nuclear transparency for the parallel kinematics. It is seen

that the gross features of the $p_{m,z}$ -dependence of the CT effect are stable with respect to variation of α_2 . In the transverse kinematics, the variation of α_2 yields only the overall renormalization of the nuclear transparency. Thus, as far as the forward-backward asymmetry of the nuclear transparency is concerned, the uncertainties of the reggeon amplitudes cannot change the situation considerably. However, we are bound to conclude that for $Q^2 \lesssim 20$ GeV² the real situation may be more complicated for the observation of CT through Q^2 -dependence of the integrated nuclear transparency.

In addition to the above discussion on the uncertainties of the theoretical predictions, it is also appropriate to comment on the off-shell effects, which are neglected in our analysis. A successful observation of the missing-momentum

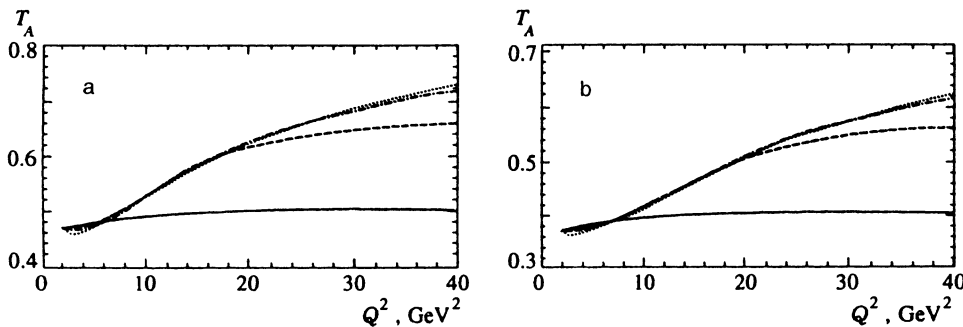


FIG. 14. The convergence of the CC-MST expectation for nuclear transparency in exclusive (a) $^{16}\text{O}(e, e'p)$ and (b) $^{40}\text{Ca}(e, e'p)$ scattering for the missing-momentum window $p_{m,\perp}, |p_{m,z}| \leq 200$ MeV/c with respect to the number of the $3q$ states included: $n=1$ (solid curve), $n=2$ (dashed curve), $n=3$ (dot-and-dash curve), $n=4$ (dotted curve).

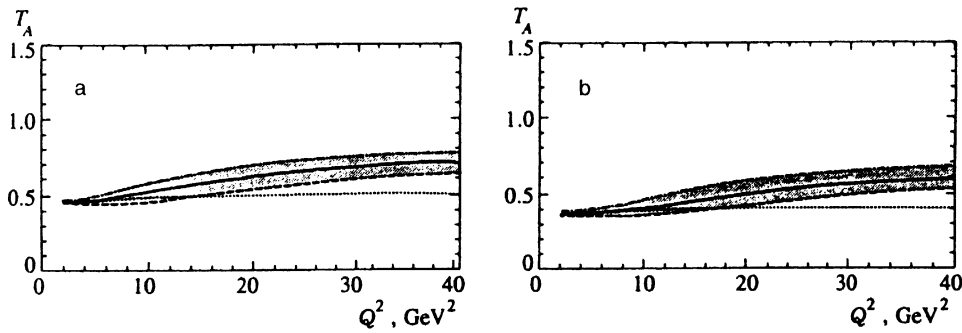


FIG. 15. Nuclear transparency for exclusive (a) $^{16}\text{O}(e, e'p)$ and (b) $^{40}\text{Ca}(e, e'p)$ scattering for the missing momentum window $p_{m\perp}, |p_{mz}| \leq 200$ MeV/c calculated within the CCMST with different sets of the reggeon parameters: $\alpha_2=0$ (solid curve), $\alpha_2=-0.5$ (dash-and-dot curve), $\alpha_2=0.5$ (dashed curve), in all the cases $\alpha_1=1$. The predictions of the Glauber model are shown by the dotted curve.

dependence of the CT effects is only possible provided that the uncertainties of the missing-momentum distribution extracted from the measured cross section of $(e, e'p)$ scattering are small in a comparison with the theoretically calculated contribution of the off-diagonal rescatterings. The determination of the missing-momentum distribution includes the division of the experimental $(e, e'p)$ cross section by the half off-shell ep cross section. As a consequence, ambiguities in σ_{ep} lead to unavoidable uncertainties in the extracted missing-momentum distribution. In order to estimate these uncertainties we compared the off-shell ep cross sections evaluated under different prescriptions discussed in Ref. 22. We found that the typical off-shell ambiguities are $\lesssim 5\text{--}10\%$ in the kinematical region considered in the present paper. Such uncertainties are not big enough to obscure the CT effects at $Q^2 \sim 10$ GeV 2 for the parallel kinematics, where CT effects increase the ratio $T_A(-p_{mz}, p_{m\perp}=0)/T_A(p_{mz}, p_{m\perp}=0)$ at $p_{mz} \sim 250$ MeV/c by the factor ~ 2 (see Figs. 2 and 3). At higher values of Q^2 ($\gtrsim 20$ GeV 2), the off-shell uncertainties can be neglected both for the parallel and transverse kinematics.

6. CONCLUSIONS

We have studied the missing-momentum dependence of the CT effects in $(e, e'p)$ scattering in the kinematical region

of $p_m \lesssim 250$ MeV/c and $Q^2 \lesssim 40$ GeV 2 . To perform such an analysis we developed a formalism based on the Glauber-Gribov multiple-scattering theory. In our calculations we describe the target nucleus in the independent particle shell model. The formalism of the CCMST was presented in a form including both the coherent and incoherent rescatterings. The coherent rescattering describes FSI in the exclusive $(e, e'p)$ reaction, when only one-hole excitations of the target nucleus are allowed, while inclusion of both the coherent and incoherent rescattering corresponds to inclusive experimental conditions involving all final states of the residual nucleus. The CT effects related to the incoherent rescattering were not considered in previous works.

We performed a qualitative analysis of the off-diagonal incoherent rescattering making use of the two-channel model. Our important observation is that, on the contrary to the case of coherent FSI, the contribution of the off-diagonal incoherent rescattering does not vanish at small energies of the struck proton. For this reason, even at low Q^2 , in the case of the inclusive reaction the Glauber model becomes unreliable for the treatment of FSI in the region of large missing momenta, where the incoherent rescattering dominates. We demonstrate that CT leads to a decrease of the contribution of the incoherent rescattering and a conspiracy of the CT effects from the coherent and incoherent rescattering may

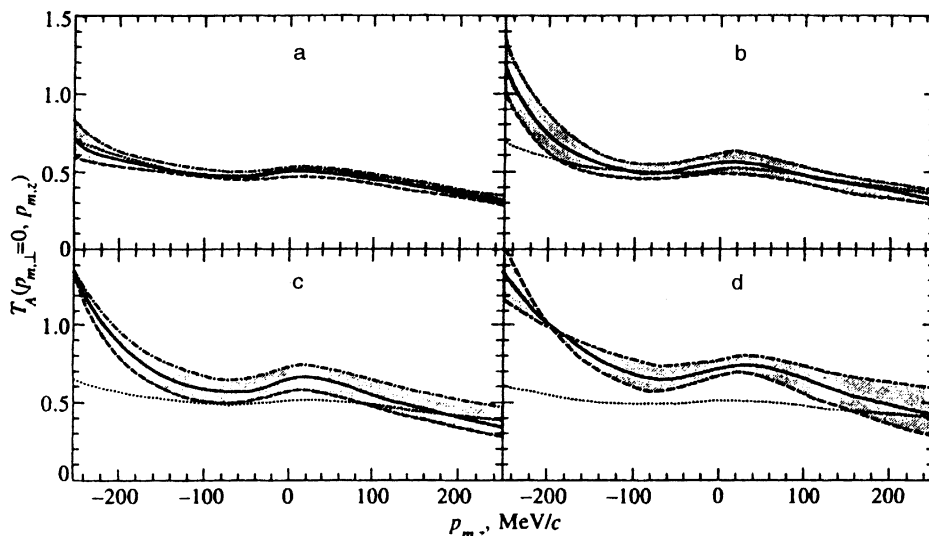


FIG. 16. The p_{mz} -dependence of the nuclear transparency for exclusive $^{16}\text{O}(e, e'p)$ scattering: (a) $Q^2=5$ GeV 2 ; (b) $Q^2=10$ GeV 2 ; (c) $Q^2=20$ GeV 2 ; (d) $Q^2=40$ GeV 2 . The legend of curves is the same as in Fig. 15.

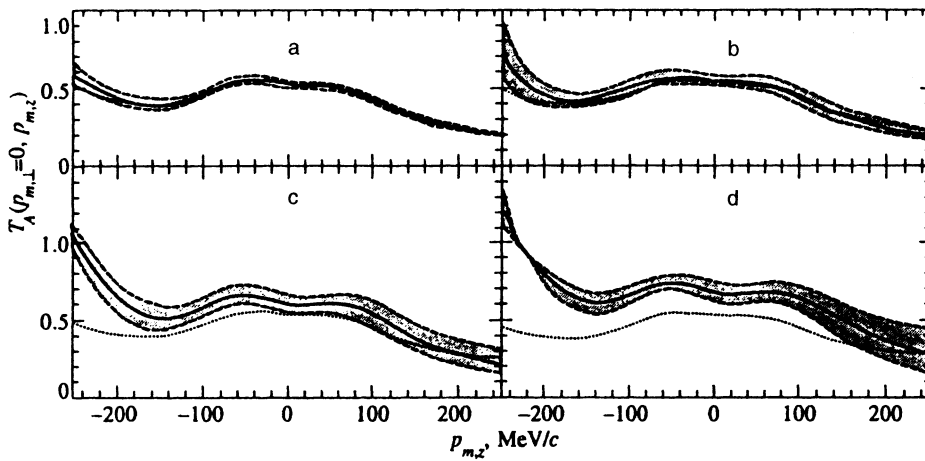


FIG. 17. The same as Fig. 16, but for $^{40}\text{Ca}(e, e'p)$ scattering.

take place in measurement of the integrated nuclear transparency. We argue that this phenomenon may be important in $(p, 2p)$ scattering, where the contribution of the incoherent rescattering is enhanced in comparison with the $(e, e'p)$ reaction.

The numerical calculations of the present paper were carried out for the exclusive $(e, e'p)$ reaction. In the region $p_m \lesssim 150\text{--}200$ MeV/c, where the effect of the incoherent FSI becomes small, our predictions may be compared with the experimental data obtained in inclusive $(e, e'p)$ reaction. Our calculations show that for $Q^2 \lesssim 5$ GeV 2 the CT effects are still small in the whole missing-momentum region considered in the present paper. For $Q^2 \sim 10$ GeV 2 , we find a considerable CT effect only in the case of the parallel kinematics in the region of $p_{m,z} \sim -(200\text{--}250)$ MeV/c. The CT increases the ratio $T_A(-p_{m,z}, p_{m,z}=0)/T_A(p_{m,z}, p_{m,z}=0)$ at $p_{m,z} \sim 250$ MeV/c by the factor ~ 2 . This effect is stronger for the light target nuclei. It could be observed in a high-precision experiment. Our calculations show that the developed CT regime starts with $Q^2 \sim 40$ GeV 2 , where the CT effects change the missing-momentum distribution drastically.

We studied for the first time the impact of the reggeon exchanges on the CT effects. It was found that in the region of $Q^2 \lesssim 40$ GeV 2 the effect of the diagonal $3q$ -nucleon reggeon amplitudes is practically saturated by the elastic $pN \rightarrow pN$ amplitude. However, the off-diagonal resonance-nucleon reggeon amplitudes may be important. We found that the onset of the CT regime for integrated nuclear transparency may be delayed if the reggeon exchanges generates a positive value of the Re/Im ratio for the off-diagonal amplitudes. Nonetheless, the CT effect in the forward-backward asymmetry is insensitive to the reggeon amplitudes.

For the first time we presented a detailed analysis of the convergence of the CCMST series in the number of the included resonance states. Our results indicate that for $Q^2 \lesssim 40$ GeV 2 the first two-three excited states practically saturate the contribution of the off-diagonal rescattering in exclusive $(e, e'p)$ scattering.

The results obtained for the integrated nuclear transparency show that the observation of CT through the

Q^2 -dependence of the integrated nuclear transparency is hardly possible for $Q^2 \lesssim 10$ GeV 2 . However, extension of the kinematical region up to $Q^2 \sim 40$ GeV 2 could permit observation of CT if the small-size $3q$ configurations actually dominate in hard ep scattering.

This work was partly supported by Grant N9S000 from the International Science Foundation and INTAS grant 93-239; the work of N.N.N. was supported by DFG grant ME864/13-1. One of the authors (A.A.U.) acknowledges A. Zichichi and ICSC-World Laboratory for financial support. One of the authors (B.G.Z.) wishes to gratefully acknowledge the hospitality of the Interdisciplinary Laboratory of SISSA and the Institut für Kernphysik, KFA, Jülich.

- ¹S. J. Brodsky and G. P. Lepage, Phys. Rev. D **22**, 2157 (1980).
- ²A. H. Mueller, in *Proceedings of the XVII Rencontre de Moriond, Les Arcs, France*, ed. by Tranh Thanh Van, Editions Frontieres, Gif-sur-Yvette (1982), p. 13.
- ³S. J. Brodsky, in *Proceedings of the XIII International Symposium on Multiparticle Dynamics, Volendam, Netherlands*, ed. by E. W. Kittel, W. Metzger, and A. Stergion, World Scientific, Singapore (1982), p. 963.
- ⁴R. J. Glauber, in *Lectures in Theoretical Physics*, Vol. 1, ed. by W. Brittain and L. G. Dunham, Interscience Publ., New York (1959); R. J. Glauber and G. Matthiae, Nucl. Phys. B **21**, 135 (1970).
- ⁵V. N. Gribov, Zh. Éksp. Teor. Fiz. **56**, 892 (1969) [Sov. Phys. JETP **29**, 483 (1969)]; Zh. Éksp. Teor. Fiz. **57**, 1306 (1970) [Sov. Phys. JETP **30**, 709 (1970)].
- ⁶N. N. Nikolaev, A. Szczurek, J. Speth *et al.*, Nucl. Phys. A **567**, 781 (1994).
- ⁷A. Bianconi, S. Boffi, and D. E. Kharzeev, Nucl. Phys. A **565**, 767 (1993).
- ⁸B. K. Jennings and B. Z. Kopeliovich, Phys. Rev. Lett. **70**, 3384 (1993).
- ⁹N. N. Nikolaev, A. Szczurek, J. Speth *et al.*, Phys. Lett. B **317**, 287 (1993).
- ¹⁰A. Bianconi, S. Boffi, and D. E. Kharzeev, Phys. Lett. B **325**, 294 (1994).
- ¹¹A. Kohama and K. Yazaki, Nucl. Phys. A **575**, 645 (1994).
- ¹²A. Kohama, K. Yazaki, and R. Seki, Phys. Lett. B **344**, 61 (1995).
- ¹³B. Z. Kopeliovich and B. G. Zakharov, Phys. Rev. D **44**, 3466 (1991).
- ¹⁴B. Z. Kopeliovich and B. G. Zakharov, Phys. Lett. B **264**, 434 (1991).
- ¹⁵NE18 Collaboration: N. C. R. Makins, R. Ent, M. S. Chapman *et al.*, Phys. Rev. Lett. **72**, 1986 (1994); T. G. O'Neill, W. Lorenzon, P. Anthony *et al.*, Phys. Lett. B **351**, 93 (1995).
- ¹⁶O. Benhar, A. Fabrocini, S. Fantoni *et al.*, Phys. Rev. C **44**, 2328 (1991).
- ¹⁷N. N. Nikolaev, J. Speth, and B. G. Zakharov, Jülich preprint KFA-IKP(Th)-1995-01, January 1995, submitted to Nucl. Phys. A.
- ¹⁸O. Benhar, S. Fantoni, N. N. Nikolaev *et al.*, Phys. Lett. B **358**, 191 (1995).
- ¹⁹J. W. Van Orden, W. Truex, and M. K. Banerjee, Phys. Rev. C **21**, 2628 (1980); S. Fantoni and V. R. Pandharipande, Nucl. Phys. A **427**, 473

- (1984); S. C. Pieper, R. B. Wiringa, and V. R. Pandharipande, *Phys. Rev. C* **46**, 1741 (1992).
- ²⁰A. Bianconi, S. Jeschonnek, N. N. Nikolaev, and B. G. Zakharov, Jülich preprint KFA-IKP(Th)-1995-13; submitted to *Nucl. Phys. A* (1996).
- ²¹F. F. Frankfurt, M. I. Strikman, and M. B. Zhalov, *Nucl. Phys. A* **515**, 599 (1990).
- ²²T. de Forest Jr., *Nucl. Phys. A* **392**, 232 (1983).
- ²³S. Frullani and J. Mourgey, in *Advanced Nuclear Physics*, ed. by J. W. Negele and E. Vogt, Plenum Press, New York-London (1984), Vol. 14, p. 3.
- ²⁴S. Boffi, C. Giusti, and F. D. Pacati, *Phys. Rep.* **226**, 1 (1993).
- ²⁵G. D. Alkhozov, S. I. Belostotsky, and A. A. Vorobyev, *Phys. Rep. C* **42**, 89 (1978).
- ²⁶B. G. Zakharov, *Yad. Fiz.* **46**, 148 (1987) [*Sov. J. Nucl. Phys.* **46**, 92 (1987)].
- ²⁷F. Low, *Phys. Rev. D* **12**, 163 (1975); S. Nussinov, *Phys. Rev. Lett.* **34**, 1286 (1975).
- ²⁸B. Z. Kopeliovich and B. G. Zakharov, *Yad. Fiz.* **46**, 1535 (1987) [*Sov. J. Nucl. Phys.* **46**, 911 (1987)].
- ²⁹N. N. Nikolaev and B. G. Zakharov, *Z. für Phys. C* **49**, 607 (1991).
- ³⁰N. N. Nikolaev and B. G. Zakharov, *Z. für Phys. C* **53**, 331 (1992).
- ³¹N. N. Nikolaev and B. G. Zakharov, in *Nuclear Physics—at the Frontiers of Knowledge (Proceedings of the International Nuclear Physics Conference, August 21–26, 1995, Beijing, China)*, ed. by Sun Zuxun and Xu Jincheng, World Scientific, Singapore - New Jersey - London - Hong Kong (1996), p. 275.
- ³²G. Alberi and G. Goggi, *Phys. Rep.* **74**, 1 (1981).
- ³³J. Nemchik, N. N. Nikolaev, and B. G. Zakharov, in *Proceedings of the Workshop on CEBAF at Higher Energies*, CEBAF, April 14–16, 1994, ed. by N. Isgur and P. Stoler, CEBAF Publ. Dept., Newport News, USA (1995), p. 415.
- ³⁴G. Cohen-Tannoudji, A. E. Hassouni, J. Kalinowski, and R. Peschanski, *Phys. Rev. D* **19**, 3397 (1979); A. Capella and J. Tran Thanh Van, *Phys. Lett. B* **114**, 450 (1982); A. B. Kaidalov, *Phys. Lett. B* **116**, 459 (1982).
- ³⁵N. N. Nikolaev, *JETP Lett.* **57**, 85 (1993).
- ³⁶H. de Vries, C. W. de Jager, and C. de Vries, *Atomic Data and Nuclear Data Tables* **36**, 496 (1987).
- ³⁷O. Benhar, C. Ciofi Degli Atti, S. Liuti, and G. Salme, *Phys. Lett. B* **177**, 135 (1986).
- ³⁸C. Lechanoine-LeLuc and F. Lehar, *Rev. Mod. Phys.* **65**, 47 (1993).

Published in English in the original Russian journal. Reproduced here with stylistic changes by the Translation Editor.